

# Using lower-redshift, non-CMB, data to constrain the Hubble constant and other cosmological parameters

Shulei Cao  <sup>1</sup>\*, Bharat Ratra  <sup>1</sup>  


<sup>1</sup>*Department of Physics, Kansas State University, 116 Cardwell Hall, Manhattan, KS 66506, USA*

Accepted XXX. Received YYY; in original form ZZZ

## ABSTRACT

We use updated Hubble parameter and baryon acoustic oscillation data, as well as other lower-redshift Type Ia supernova, Mg II reverberation-measured quasar, quasar angular size, H II starburst galaxy, and Amati-correlated gamma-ray burst data, to jointly constrain cosmological parameters in six cosmological models. The joint analysis provides model-independent determinations of the Hubble constant,  $H_0 = 69.7 \pm 1.2 \text{ km s}^{-1} \text{ Mpc}^{-1}$ , and the current non-relativistic matter density parameter,  $\Omega_{m0} = 0.295 \pm 0.017$ . These error bars are factors of 2.2 and 2.3 larger than the corresponding error bars in the flat  $\Lambda$ CDM model from *Planck* TT,TE,EE+lowE+lensing cosmic microwave background anisotropy data. Based on the deviance information criterion (DIC), the flat  $\Lambda$ CDM model is most favored but mild dark energy dynamics and a little spatial curvature are not ruled out.

**Key words:** cosmological parameters – dark energy – cosmology: observations – gamma-ray bursts

## 1 INTRODUCTION

The expansion of the Universe is currently accelerating. This is well-supported by many observations but the underlying theory remains obscure. If general relativity is valid on cosmological scales, a dark energy that has negative pressure is thought to be responsible for the accelerated cosmological expansion. In the well-known spatially-flat  $\Lambda$ CDM model (Peebles 1984), dark energy is a cosmological constant  $\Lambda$  and contributes  $\sim 70\%$  of the current cosmological energy budget (see, e.g. Farooq et al. 2017; Scolnic et al. 2018; Planck Collaboration 2020; eBOSS Collaboration 2021). However, potential observational discrepancies (see, e.g. Di Valentino et al. 2021b; Perivolaropoulos & Skara 2021; Abdalla et al. 2022) motivate consideration of other cosmological models besides flat  $\Lambda$ CDM. In our analyses here we also allow for non-zero spatial curvature<sup>1</sup> as well as dark energy dynamics.

Many observations have been used to compare the goodness of fit of cosmological models and determine cosmological parameter constraints. These include CMB anisotropy data (see, e.g. Planck Collaboration 2020) that largely probe the high-redshift,  $z \sim 1100$ , Universe, as well as lower- $z$  cos-

mological measurements that we make use of here, such as reverberation-measured H $\beta$  quasar (QSO) and Mg II QSO observations that reach to  $z \sim 1.9$  (see, e.g. Czerny et al. 2021; Zajaček et al. 2021; Yu et al. 2021; Khadka et al. 2021b,a),<sup>2</sup> Hubble parameter [ $H(z)$ ] data that reach to  $z \sim 2$  (see, e.g. Moresco et al. 2016; Farooq et al. 2017; Ryan et al. 2019; Cao et al. 2022b), type Ia supernova (SN Ia) observations that reach to  $z \sim 2.3$  (see, e.g. Scolnic et al. 2018; DES Collaboration 2019c), baryon acoustic oscillation (BAO) measurements that reach to  $z \sim 2.3$  (see, e.g. eBOSS Collaboration 2021; Cao et al. 2022b), H II starburst galaxy apparent magnitude data that reach to  $z \sim 2.4$  (see, e.g. Mania & Ratra 2012; Chávez et al. 2014; González-Morán et al. 2021; Cao et al. 2022b; Johnson et al. 2022; Mehrabi et al. 2022), QSO angular size (QSO-AS) measurements that reach to  $z \sim 2.7$  (see, e.g. Cao et al. 2017; Ryan et al. 2019; Cao et al. 2020, 2022b; Zheng et al. 2021; Lian et al. 2021), QSO flux observations that reach to  $z \sim 7.5$  (Risaliti & Lusso 2015, 2019; Khadka & Ratra 2020a,b, 2021, 2022; Lusso et al. 2020; Yang et al. 2020; Zhao & Xia 2021; Li et al. 2021; Lian et al. 2021; Luongo et al. 2021; Rezaei

\* E-mail: shulei@phys.ksu.edu

† E-mail: ratra@phys.ksu.edu

<sup>1</sup> The *Planck* TT,TE,EE+lowE+lensing cosmic microwave background (CMB) anisotropy data favor positive spatial curvature over flatness (Planck Collaboration 2020).

<sup>2</sup> Current H $\beta$  QSO data probe to  $z \sim 0.9$  and the resulting cosmological parameter constraints from these data are in  $\sim 2\sigma$  tension with those from better-established cosmological probes (Khadka et al. 2021a) so we do not use these data in our analyses here.

et al. 2022; Dainotti et al. 2022a),<sup>3</sup> and gamma-ray burst (GRB) data that reach to  $z \sim 8.2$  (see, e.g. Wang et al. 2016, 2022; Dainotti et al. 2016, 2017, 2020; Fana Dirirsa et al. 2019; Amati et al. 2019; Khadka & Ratra 2020c; Hu et al. 2021; Dai et al. 2021; Demianski et al. 2021; Khadka et al. 2021c; Luongo & Muccino 2021; Cao et al. 2022c,d,a; Liu et al. 2022; Dainotti et al. 2022b).<sup>4</sup>

In this paper, we use most of the aforementioned non-CMB data sets to jointly constrain cosmological parameters. In Cao et al. (2021b), by using  $H(z)$  + BAO + SN data (SN refers to Pantheon and DES-3yr SN Ia data, discussed in Sec. 3 below), we estimated summary values of the current non-relativistic matter density parameter  $\Omega_{m0} = 0.294 \pm 0.020$  and the Hubble constant  $H_0 = 68.8 \pm 1.8 \text{ km s}^{-1} \text{ Mpc}^{-1}$ . In Cao et al. (2022b), by using  $H(z)$  + BAO + SN + QSO-AS + H II G data, summary values of  $\Omega_{m0} = 0.293 \pm 0.021$  and  $H_0 = 69.7 \pm 1.2 \text{ km s}^{-1} \text{ Mpc}^{-1}$  were obtained. Compared to our earlier analysis, the addition of QSO-AS and H II G data results in similar constraints on  $\Omega_{m0}$  with a slightly larger  $1\sigma$  uncertainty and more restrictive ( $1\sigma$  uncertainty reduced by 50%)  $H_0$  constraints, with a higher central value of  $H_0$  ( $0.42\sigma$  higher).

In our analysis here we improve on our earlier work by more correctly accounting for the neutrinos. We also use updated BAO and  $H(z)$  data and now also include Mg II QSO and A118 GRB data.<sup>5</sup> Here the joint analyses of  $H(z)$  + BAO + SN + QSO-AS + H II G + Mg II QSO + A118 data provide model-independent values of  $\Omega_{m0} = 0.295 \pm 0.017$  and  $H_0 = 69.7 \pm 1.2 \text{ km s}^{-1} \text{ Mpc}^{-1}$ . Our  $H_0$  measurement is in better agreement with the median statistics  $H_0$  estimate of Chen & Ratra (2011) than with the local expansion rate  $H_0$  estimate of Riess et al. (2021). Flat  $\Lambda$ CDM is favored the most, but mild dark energy dynamics or a little spatial curvature energy density is not ruled out. Although here we use updated  $H(z)$  and BAO data, and add Mg II QSO and A118 data, the constraint on  $H_0$  is identical to that of Cao et al. (2022b),<sup>6</sup> whereas the new constraint on  $\Omega_{m0}$  is more restrictive ( $1\sigma$  uncertainty reduced by  $\sim 24\%$ ) and  $\sim 0.15\sigma$  higher.

This paper is organized as follows. In Sec. 2 we introduce the cosmological models/parametrizations used in our analyses. In Sec. 3 we describe the data sets used in our analyses, with the methods we use summarized in Sec. 4.

<sup>3</sup> We do not use these data in this paper since the latest Lusso et al. (2020) QSO flux compilation assumes a UV–X-ray correlation model that is invalid above  $z \sim 1.5 - 1.7$  (Khadka & Ratra 2021, 2022).

<sup>4</sup> Only a subset containing 118 Amati-correlated GRBs are suitable for cosmological purposes (Khadka & Ratra 2020c; Cao et al. 2021a; Khadka et al. 2021c), and these are the Amati-correlated GRBs we use in our analyses here.

<sup>5</sup> We also examined constraints from mutually consistent Platinum + A101 GRB data used in Cao et al. (2022d) and jointly analyzed them with QSO-AS, H II G, and Mg II QSO data. Cosmological constraints from the joint QSO-AS + H II G + Mg II QSO + Platinum + A101 data are similar to those from the QSO-AS + H II G + Mg II QSO + A118 data, so we decided to perform further analyses with the latter that constrain fewer non-cosmological parameters.

<sup>6</sup> Mg II QSO and A118 data do not have the power to constrain  $H_0$  and updated  $H(z)$  and BAO data we use here provide similar constraints to those from older BAO and  $H(z)$  data.

We discuss our cosmological parameter constraints results in Sec. 5 and summarize our conclusions in Sec. 6.

## 2 COSMOLOGICAL MODELS

In this paper, we use various combinations of data to constrain cosmological model parameters in six spatially-flat and non-flat dark energy cosmological models.<sup>7</sup> Using a number of different models allows us to determine which results are less dependent on the model used to derive them. The expansion rate,  $E(z, \mathbf{p})$ , as a function of redshift  $z$  and the cosmological parameters  $\mathbf{p}$  in a given cosmological model, is defined as  $E(z, \mathbf{p}) \equiv H(z, \mathbf{p})/H_0$ , with  $H(z, \mathbf{p})$  being the Hubble parameter. The expansion rate is used to compute cosmological-parameter-dependent predictions in the cosmological models we study. In these cosmological models, as in Cao et al. (2022d), we assume one massive and two massless neutrino species, with the effective number of relativistic neutrino species  $N_{\text{eff}} = 3.046$  and the total neutrino mass  $\sum m_\nu = 0.06 \text{ eV}$ . Therefore, here the current value of the non-relativistic neutrino physical energy density parameter,  $\Omega_\nu h^2 = \sum m_\nu / (93.14 \text{ eV})$ , is not a free parameter, and along with the current values of the observationally-constrained baryonic ( $\Omega_b h^2$ ) and cold dark matter ( $\Omega_c h^2$ ) physical energy density parameters,  $\Omega_{m0}$  is derived as  $\Omega_{m0} = (\Omega_\nu h^2 + \Omega_b h^2 + \Omega_c h^2)/h^2$ , where  $h$  is the Hubble constant in units of  $100 \text{ km s}^{-1} \text{ Mpc}^{-1}$ .

In the  $\Lambda$ CDM models the expansion rate function is

$$E(z, \mathbf{p}) = \sqrt{\Omega_{m0} (1+z)^3 + \Omega_{k0} (1+z)^2 + \Omega_\Lambda}, \quad (1)$$

where  $\Omega_\Lambda = 1 - \Omega_{m0} - \Omega_{k0}$  is the cosmological constant dark energy density parameter,  $\Omega_{k0}$  is the current value of the spatial curvature energy density parameter, and  $\Omega_{k0} = 0$  implies flat spatial hypersurfaces. The cosmological parameters  $\mathbf{p} = \{H_0, \Omega_b h^2, \Omega_c h^2\}$  and  $\mathbf{p} = \{H_0, \Omega_b h^2, \Omega_{c0} h^2, \Omega_{k0}\}$  are constrained in the flat and non-flat  $\Lambda$ CDM models, respectively. Note that when  $H_0$  and  $\Omega_b h^2$  are fixed in analyses of some of the data sets we use,  $\mathbf{p}$  change accordingly.

In the XCDM parametrizations,

$$E(z, \mathbf{p}) = \sqrt{\Omega_{m0} (1+z)^3 + \Omega_{k0} (1+z)^2 + \Omega_{X0} (1+z)^{3(1+w_X)}}, \quad (2)$$

where  $w_X$  is the X-fluid equation of state parameter, and  $\Omega_{X0} = 1 - \Omega_{m0} - \Omega_{k0}$  is the current value of the X-fluid dynamical dark energy density parameter. The cosmological parameters  $\mathbf{p} = \{H_0, \Omega_b h^2, \Omega_c h^2, w_X\}$  and  $\mathbf{p} = \{H_0, \Omega_b h^2, \Omega_{c0} h^2, w_X, \Omega_{k0}\}$  are constrained in the flat and non-flat XCDM parametrizations, respectively. When  $w_X = -1$  the XCDM parametrization reduces to the  $\Lambda$ CDM model.

<sup>7</sup> For recent determinations of constraints on spatial curvature, see Chen et al. (2016), Rana et al. (2017), Ooba et al. (2018a,c), Yu et al. (2018), Park & Ratra (2019c,a), Wei (2018), DES Collaboration (2019a), Li et al. (2020), Handley (2019), Efstathiou & Gratton (2020), Di Valentino et al. (2021a), Vagnozzi et al. (2021a,b), KiDS Collaboration (2021), Arjona & Nesseris (2021), Dhawan et al. (2021), Renzi et al. (2022), Geng et al. (2022), Wei & Melia (2022), Mukherjee & Banerjee (2022), and references therein.

In the  $\phi$ CDM models (Peebles & Ratra 1988; Ratra & Peebles 1988; Pavlov et al. 2013),<sup>8</sup>

$$E(z, \mathbf{p}) = \sqrt{\Omega_{m0}(1+z)^3 + \Omega_{k0}(1+z)^2 + \Omega_\phi(z, \alpha)}, \quad (3)$$

where

$$\Omega_\phi(z, \alpha) = \frac{1}{6H_0^2} \left[ \frac{1}{2}\dot{\phi}^2 + V(\phi) \right], \quad (4)$$

is the scalar field ( $\phi$ ) dynamical dark energy density parameter and is determined by numerically solving the Friedmann equation (3) and the equation of motion of the scalar field

$$\ddot{\phi} + 3H\dot{\phi} + V'(\phi) = 0. \quad (5)$$

An inverse power-law scalar field potential energy density is assumed as

$$V(\phi) = \frac{1}{2}\kappa m_p^2 \phi^{-\alpha}. \quad (6)$$

In the preceding equations an overdot and a prime denote a derivative with respect to time and  $\phi$ , respectively,  $m_p$  is the Planck mass,  $\alpha$  is a positive constant (when  $\alpha = 0$   $\phi$ CDM reduces to  $\Lambda$ CDM), and  $\kappa$  is a constant that is determined by the shooting method in the Cosmic Linear Anisotropy Solving System (CLASS) code (Blas et al. 2011). The cosmological parameters  $\mathbf{p} = \{H_0, \Omega_b h^2, \Omega_c h^2, \alpha\}$  and  $\mathbf{p} = \{H_0, \Omega_b h^2, \Omega_c h^2, \alpha, \Omega_{k0}\}$  are constrained in the flat and non-flat  $\phi$ CDM models, respectively.

### 3 DATA

In this paper we use updated  $H(z)$  and BAO data, as well as other data sets, to constrain cosmological parameters. These are summarized next.

**$H(z)$  data.** There are 32  $H(z)$  measurements listed in Table 1, spanning the redshift range  $0.07 \leq z \leq 1.965$ . Compared with what is given in table 1 of Ryan et al. (2018), the updated  $H(z)$  data here have one additional data point from Borghi et al. (2022).

**BAO data.** There are 12 BAO measurements listed in Table 2, spanning the redshift range  $0.122 \leq z \leq 2.334$ . The covariance matrices for given BAO data are summarized below.

The covariance matrix  $\mathbf{C}$  for BAO data from du Mas des Bourboux et al. (2020) is

$$\begin{bmatrix} 1.3225 & -0.1009 \\ -0.1009 & 0.0380 \end{bmatrix}, \quad (7)$$

for BAO data from Gil-Marín et al. (2020)  $\mathbf{C}$  is

$$\begin{bmatrix} 0.02860520 & -0.04939281 & 0.01489688 & -0.01387079 \\ -0.04939281 & 0.5307187 & -0.02423513 & 0.1767087 \\ 0.01489688 & -0.02423513 & 0.04147534 & -0.04873962 \\ -0.01387079 & 0.1767087 & -0.04873962 & 0.3268589 \end{bmatrix}, \quad (8)$$

<sup>8</sup> For recent determinations of constraints on  $\phi$ CDM see Zhai et al. (2017), Ooba et al. (2018b, 2019), Park & Ratra (2018, 2019b, 2020), Sangwan et al. (2018), Solà Peracaula et al. (2019), Singh et al. (2019), Ureña-López & Roy (2020), Sinha & Banerjee (2021), Xu et al. (2021), de Cruz Perez et al. (2021), Jesus et al. (2021), and references therein.

**Table 1.** Updated  $H(z)$  data.

$z$	$H(z)$ <sup>a</sup>	Reference
0.07	$69.0 \pm 19.6$	Zhang et al. (2014)
0.09	$69.0 \pm 12.0$	Simon et al. (2005)
0.12	$68.6 \pm 26.2$	Zhang et al. (2014)
0.17	$83.0 \pm 8.0$	Simon et al. (2005)
0.179	$75.0 \pm 4.0$	Moresco et al. (2012)
0.199	$75.0 \pm 5.0$	Moresco et al. (2012)
0.2	$72.9 \pm 29.6$	Zhang et al. (2014)
0.27	$77.0 \pm 14.0$	Simon et al. (2005)
0.28	$88.8 \pm 36.6$	Zhang et al. (2014)
0.352	$83.0 \pm 14.0$	Moresco et al. (2012)
0.3802	$83.0 \pm 13.5$	Moresco et al. (2016)
0.4	$95.0 \pm 17.0$	Simon et al. (2005)
0.4004	$77.0 \pm 10.2$	Moresco et al. (2016)
0.4247	$87.1 \pm 11.2$	Moresco et al. (2016)
0.4497	$92.8 \pm 12.9$	Moresco et al. (2016)
0.47	$89.0 \pm 50.0$	Ratsimbazafy et al. (2017)
0.4783	$80.9 \pm 9.0$	Moresco et al. (2016)
0.48	$97.0 \pm 62.0$	Stern et al. (2010)
0.593	$104.0 \pm 13.0$	Moresco et al. (2012)
0.68	$92.0 \pm 8.0$	Moresco et al. (2012)
0.75	$98.8 \pm 33.6$	Borghi et al. (2022)
0.781	$105.0 \pm 12.0$	Moresco et al. (2012)
0.875	$125.0 \pm 17.0$	Moresco et al. (2012)
0.88	$90.0 \pm 40.0$	Stern et al. (2010)
0.9	$117.0 \pm 23.0$	Simon et al. (2005)
1.037	$154.0 \pm 20.0$	Moresco et al. (2012)
1.3	$168.0 \pm 17.0$	Simon et al. (2005)
1.363	$160.0 \pm 33.6$	Moresco (2015)
1.43	$177.0 \pm 18.0$	Simon et al. (2005)
1.53	$140.0 \pm 14.0$	Simon et al. (2005)
1.75	$202.0 \pm 40.0$	Simon et al. (2005)
1.965	$186.5 \pm 50.4$	Moresco (2015)

<sup>a</sup> km s<sup>-1</sup> Mpc<sup>-1</sup>.

**Table 2.** Updated BAO data.

$z$	Measurement <sup>a</sup>	Value	Reference
0.122	$D_V(r_s, \text{fid}/r_s)$	$539 \pm 17$	Carter et al. (2018)
0.38	$D_M/r_s$	10.23406	Gil-Marín et al. (2020) <sup>b</sup>
0.38	$D_H/r_s$	24.98058	Gil-Marín et al. (2020) <sup>b</sup>
0.51	$D_M/r_s$	13.36595	Gil-Marín et al. (2020) <sup>b</sup>
0.51	$D_H/r_s$	22.31656	Gil-Marín et al. (2020) <sup>b</sup>
0.698	$D_M/r_s$	17.85823691865007	c
0.698	$D_H/r_s$	19.32575373059217	c
0.81	$D_A/r_s$	$10.75 \pm 0.43$	DES Collaboration (2019b)
1.48	$D_M/r_s$	30.6876	d
1.48	$D_H/r_s$	13.2609	d
2.334	$D_M/r_s$	37.5	e
2.334	$D_H/r_s$	8.99	e

<sup>a</sup>  $D_V, r_s, r_s, \text{fid}, D_M, D_H$ , and  $D_A$  have units of Mpc.

<sup>b</sup> The four measurements from Gil-Marín et al. (2020) are correlated; see equation (8) for their correlation matrix.

<sup>c</sup> The two measurements from Gil-Marín et al. (2020) and Bautista et al. (2021) are correlated; see equation (9) for their correlation matrix.

<sup>d</sup> The two measurements from Neveux et al. (2020) and Hou et al. (2021) are correlated; see equation (10) for their correlation matrix.

<sup>e</sup> The two measurements from du Mas des Bourboux et al. (2020) are correlated; see equation (7) for their correlation matrix.

for BAO data from Gil-Marín et al. (2020) and Bautista et al. (2021)  $\mathbf{C}$  is

$$\begin{bmatrix} 0.1076634008565565 & -0.05831820341302727 \\ -0.05831820341302727 & 0.2838176386340292 \end{bmatrix}, \quad (9)$$

and for BAO data from Neveux et al. (2020) and Hou et al. (2021)  $\mathbf{C}$  is

$$\begin{bmatrix} 0.63731604 & 0.1706891 \\ 0.1706891 & 0.30468415 \end{bmatrix}. \quad (10)$$

**SN Ia data.** As in Cao et al. (2022b), we use SN Ia data that consist of 1048 Pantheon (Scolnic et al. 2018) and 20 binned DES 3yr (DES Collaboration 2019c) SNe Ia, span-

ning the redshift ranges  $0.01 < z < 2.3$  and  $0.015 \leq z \leq 0.7026$ , respectively.

**QSO angular size (QSO-AS) data.** There are 120 QSO-AS measurements listed in table 1 of Cao et al. (2017), spanning the redshift range  $0.462 \leq z \leq 2.73$ . The measured quantities are  $z$  and the angular size  $\theta(z)$  with the characteristic linear size of QSOs in the sample,  $l_m$ , as a free parameter to be constrained. The angular size  $\theta(z) = l_m/D_A(z)$ , where  $D_A(z)$  is the angular diameter distance. A detailed description of the use of these data can be found in Cao et al. (2022b).

**H II G data.** There are 181 H II G measurements listed in table A3 of González-Morán et al. (2021), with 107 low- $z$  data from Chávez et al. (2014) recalibrated by González-Morán et al. (2019), spanning the redshift range  $0.0088 \leq z \leq 0.16417$ , and 74 high- $z$  data spanning the redshift range  $0.63427 \leq z \leq 2.545$ . The measured quantities are  $z$ , H II G flux  $F(\text{H}\beta)$ , and velocity dispersion  $\sigma$ .

**Mg II QSO sample.** The Mg II QSO sample consists of 78 QSOs listed in table A1 of Khadka et al. (2021b), spanning the redshift range  $0.0033 \leq z \leq 1.89$ . Mg II QSO data obey the radius-luminosity ( $R - L$ ) relation and the measured quantities are the time delay  $\tau$  and QSO flux  $F_{3000}$  measured at 3000 Å.

**A118 sample.** The A118 sample includes 118 long GRBs listed in table 7 of Khadka et al. (2021c), spanning the redshift range  $0.3399 \leq z \leq 8.2$ . A118 data obey the Amati (or  $E_p - E_{\text{iso}}$ ) correlation and the measured quantities are  $z$ , rest-frame spectral peak energy  $E_p$ , and measured bolometric fluence  $S_{\text{bolo}}$ , computed in the standard rest-frame energy band  $1 - 10^4$  keV.<sup>9</sup>

**Platinum + A101 sample.** The Platinum sample includes 50 long GRBs listed in table A1 of Cao et al. (2022d), spanning the redshift range  $0.553 \leq z \leq 5.0$ . The A101 sample includes 101 long GRBs with common GRBs between the Platinum and the A118 samples excluded, spanning the redshift range  $0.3399 \leq z \leq 8.2$ . The Platinum GRBs obey the three-dimensional Dainotti correlation and the measured quantities are  $z$ , characteristic time scale  $T_X^*$ , the measured  $\gamma$ -ray energy flux  $F_X$  at  $T_X^*$ , the prompt peak flux  $F_{\text{peak}}$  over a 1 s interval, and the X-ray spectral index of the plateau phase  $\beta'$ .

## 4 DATA ANALYSIS METHODOLOGY

In this paper we determine constraints on the cosmological model parameters, and non-cosmological parameters related to different data sets, by maximizing the likelihood function,  $\mathcal{L}$ . These analyses are performed by using the Markov chain Monte Carlo (MCMC) code MONTEPYTHON (Audren et al.

<sup>9</sup> As noted in Liu et al. (2022), the  $E_p$  value for GRB081121 reported in table 5 of Fana Dirirsa et al. (2019), and used in our analysis here, is incorrect. One should instead use the correct value provided in table 4 of Wang et al. (2016),  $E_p = 871 \pm 123$  keV. However, since this data point has negligible effect on the cosmological-model and GRB-correlation parameter constraints and the conclusions remain unchanged after correcting it, we do not revise our Amati-correlated GRB results here and in Cao et al. (2021a, 2022c,d). In future analyses we will use the correct Wang et al. (2016) value.

**Table 3.** Flat priors of the constrained parameters.

Parameter	Prior
Cosmological Parameters	
$H_0$ <sup>a</sup>	[None, None]
$\Omega_b h^2$ <sup>b</sup>	[0, 1]
$\Omega_c h^2$ <sup>c</sup>	[0, 1]
$\Omega_{k0}$	[-2, 2]
$\alpha$	[0, 10]
$w_X$	[-5, 0.33]
Non-Cosmological Parameters	
$k$	[0, 5]
$b_M$	[0, 10]
$\sigma_{\text{int}}$	[0, 5]
$a$	[-5, 5]
$b_P$	[-5, 5]
$C_o$	[-50, 50]
$\beta$	[0, 5]
$\gamma$	[0, 300]
$l_m$	[None, None]

<sup>a</sup> km s<sup>-1</sup> Mpc<sup>-1</sup>. In the Mg II QSO + A118 case,  $H_0$  is set to be 70 km s<sup>-1</sup> Mpc<sup>-1</sup>, while in other cases, the prior range is irrelevant (unbounded).

<sup>b</sup> In the Mg II QSO + A118 case,  $\Omega_b h^2$  is set to be 0.0245, i.e.  $\Omega_b = 0.05$ .

<sup>c</sup> In the Mg II QSO + A118 case,  $\Omega_{m0} \in [0, 1]$  is ensured.

2013), with the physics coded in the CLASS code. In Table 3, we list the flat prior ranges of the constrained free parameters.

The detailed descriptions for the likelihood functions of  $H(z)$ , BAO, H II G, QSO-AS, and SN Ia data can be found in Cao et al. (2020, 2021b,a), whereas those of Platinum, A118/A101, and Mg II QSO data can be found in Cao et al. (2022d) and Khadka et al. (2021b). One can also find the definitions of the Akaike Information Criterion (AIC) and the Bayesian Information Criterion (BIC) as well as the deviance information criterion (DIC) in Cao et al. (2022d).<sup>10</sup> We compute  $\Delta\text{AIC}$ ,  $\Delta\text{BIC}$ , and  $\Delta\text{DIC}$  differences for the other five cosmological models relative to the flat  $\Lambda$ CDM reference model values. Negative (positive) values of  $\Delta\text{AIC}$ ,  $\Delta\text{BIC}$ , or  $\Delta\text{DIC}$  indicate that the model under investigation fits the data compilation better (worse) than does the reference model. Relative to the model with minimum AIC(BIC/DIC),  $\Delta\text{AIC(BIC/DIC)} \in (0, 2]$  is defined to be weak evidence against the model under investigation,  $\Delta\text{AIC(BIC/DIC)} \in (2, 6]$  is positive evidence against the model under investigation,  $\Delta\text{AIC(BIC/DIC)} \in (6, 10]$  is strong evidence against the model under investigation, and  $\Delta\text{AIC(BIC/DIC)} > 10$  is very strong evidence against the model under investigation.

## 5 RESULTS

The posterior one-dimensional probability distributions and two-dimensional confidence regions of the cosmological and non-cosmological parameters are shown in Figs. 1–6, in red

<sup>10</sup> Unlike AIC and BIC, DIC estimates the effective number of free parameters.

(QSO-AS + H II G and  $H(z) + \text{BAO} + \text{SN}$ ), green (QSO-AS + H II G + Mg II QSO + A118), orange (Mg II QSO + A118 and QSO-AS + H II G + Mg II QSO + Platinum + A101, QHMPA101), and blue ( $H(z) + \text{BAO} + \text{SN} + \text{QSO-AS} + \text{H II G} + \text{Mg II QSO} + \text{A118}$ , HzBSNQHMA). The unmarginalized best-fitting parameter values, as well as the corresponding  $-2 \ln \mathcal{L}_{\max}$ , AIC, BIC, DIC,  $\Delta \text{AIC}$ ,  $\Delta \text{BIC}$ , and  $\Delta \text{DIC}$  values, for all models and data combinations, are listed in Table 4, whereas the marginalized posterior mean parameter values and uncertainties ( $\pm 1\sigma$  error bars or  $2\sigma$  limits), for all models and data combinations, are listed in Table 5.<sup>11</sup>

In the non-flat  $\Lambda$ CDM and flat and non-flat  $\phi$ CDM models, Mg II QSO + A118 data mildly favor currently decelerating cosmological expansion, which is most likely caused by the choice of fixed  $\Omega_b$  and  $H_0$  values. All other data combinations more favor currently accelerating cosmological expansion.

### 5.1 Constraints from $H(z)$ , BAO, and SN Ia data

The updated  $H(z) + \text{BAO}$  results derived here are quite similar to the  $H(z) + \text{BAO}$  results given in Cao et al. (2022d), so we do not discuss them in detail.  $H(z) + \text{BAO} + \text{SN}$  is a more important data combination, so here we discuss these constraints in more detail. While the computation of the  $H(z) + \text{BAO} + \text{SN}$  results reported in Cao et al. (2022b) neglected the late-time contribution of non-relativistic neutrinos, in this paper, where we account for the contributions of one massive and two massless neutrino species, we find very similar constraints.

The constraints from  $H(z) + \text{BAO} + \text{SN}$  data on  $\Omega_{m0}$  range from a low of  $0.287 \pm 0.017$  (flat  $\phi$ CDM) to a high of  $0.304^{+0.014}_{-0.015}$  (flat  $\Lambda$ CDM), with a difference of  $0.75\sigma$ .

The  $H_0$  constraints range from a low of  $68.29 \pm 1.78$   $\text{km s}^{-1} \text{Mpc}^{-1}$  (flat  $\phi$ CDM) to a high of  $69.04 \pm 1.77$   $\text{km s}^{-1} \text{Mpc}^{-1}$  (flat  $\Lambda$ CDM), with a difference of  $0.30\sigma$ , which are  $0.09\sigma$  (flat  $\phi$ CDM) and  $0.31\sigma$  (flat  $\Lambda$ CDM) higher than the median statistics estimate of  $H_0 = 68 \pm 2.8$   $\text{km s}^{-1} \text{Mpc}^{-1}$  (Chen & Ratra 2011), and  $2.23\sigma$  (flat  $\phi$ CDM) and  $1.89\sigma$  (flat  $\Lambda$ CDM) lower than the local Hubble constant measurement of  $H_0 = 73.2 \pm 1.3 \text{ km s}^{-1} \text{ Mpc}^{-1}$  (Riess et al. 2021).

The constraints on  $\Omega_{k0}$  are  $0.040 \pm 0.070$ ,  $-0.001 \pm 0.098$ , and  $-0.038^{+0.071}_{-0.085}$  for non-flat  $\Lambda$ CDM, XCDM, and  $\phi$ CDM, respectively. Although non-flat hypersurfaces are mildly favored, flat hypersurfaces are well within  $1\sigma$ .

There is a slight preference for dark energy dynamics. For flat (non-flat) XCDM,  $w_X = -0.941 \pm 0.064$  ( $w_X = -0.948^{+0.098}_{-0.068}$ ), with central values being  $0.92\sigma$  ( $0.76\sigma$ ) higher than  $w_X = -1$ ; and for flat (non-flat)  $\phi$ CDM,  $\alpha = 0.324^{+0.122}_{-0.264}$  ( $\alpha = 0.382^{+0.151}_{-0.299}$ ), with central values being  $1.23\sigma$  ( $1.28\sigma$ ) away from  $\alpha = 0$ .

### 5.2 Constraints from QSO-AS, H II G, Mg II QSO, A118, and Platinum + A101 data

Given our improved treatment of neutrinos in this paper, compared to our earlier analyses, we have reanalyzed data we had previously studied.

As shown in Cao et al. (2022b), QSO-AS data alone do not deal well with  $H_0$ , so an unbounded prior range for  $H_0$  makes it hard for the computation to converge and results in an unreasonably high  $H_0$  value and so an unreasonably low  $l_m$  value. However, we expect constraints on the other cosmological parameters consistent with those given in Cao et al. (2022b). Constraints from H II G data are consistent with what are given in Cao et al. (2022b). Constraints from Mg II QSO data are consistent with those described in Khadka et al. (2021b) while those from A118 and Platinum + A101 data are consistent with those in Cao et al. (2022d). We find that cosmological parameter constraints from those four data sets are mutually consistent so they can be used to do joint analyses. As expected, cosmological parameter constraints from the joint QSO-AS + H II G data and Mg II QSO + A118 data are indeed mutually consistent, as seen in Tables 4 and 5. We do not discuss these results in detail since there are no significant changes compared to those derived in our earlier analyses. We consider the joint analyses results of QSO-AS + H II G + Mg II QSO + A118 data to be more useful and discuss these in more detail next.<sup>12</sup>

The constraints from QSO-AS + H II G + Mg II QSO + A118 data on  $\Omega_{m0}$  range from a low of  $0.175^{+0.075}_{-0.081}$  (flat  $\phi$ CDM) to a high of  $0.314^{+0.051}_{-0.044}$  (flat XCDM), with a difference of  $1.60\sigma$ . Following the pattern of H II G data, the  $\Omega_{m0}$  difference is relatively large.

The  $H_0$  constraints range from a low of  $70.38 \pm 1.84$   $\text{km s}^{-1} \text{Mpc}^{-1}$  (non-flat  $\phi$ CDM) to a high of  $73.14^{+2.14}_{-2.48}$   $\text{km s}^{-1} \text{Mpc}^{-1}$  (flat XCDM), with a difference of  $0.89\sigma$ , which are  $0.71\sigma$  (non-flat  $\phi$ CDM) and  $1.37\sigma$  (flat XCDM) higher than the median statistics estimate of  $H_0 = 68 \pm 2.8$   $\text{km s}^{-1} \text{Mpc}^{-1}$  (Chen & Ratra 2011), and  $1.25\sigma$  (non-flat  $\phi$ CDM) and  $0.02\sigma$  (flat XCDM) lower than the local Hubble constant measurement of  $H_0 = 73.2 \pm 1.3 \text{ km s}^{-1} \text{ Mpc}^{-1}$  (Riess et al. 2021).

The constraints on  $\Omega_{k0}$  are  $-0.139^{+0.116}_{-0.228}$ ,  $0.054^{+0.227}_{-0.238}$ , and  $0.044^{+0.104}_{-0.256}$  for non-flat  $\Lambda$ CDM, XCDM, and  $\phi$ CDM, respectively. As opposed to  $H(z) + \text{BAO} + \text{SN}$  results, non-flat  $\Lambda$ CDM mildly favors closed hypersurfaces, whereas non-flat XCDM and non-flat  $\phi$ CDM mildly favor open hypersurfaces. However, flat hypersurfaces are well within  $1\sigma$ .

There are mild preferences for dark energy dynamics. For flat (non-flat) XCDM,  $w_X = -1.836^{+0.804}_{-0.419}$  ( $w_X = -2.042^{+1.295}_{-0.451}$ ), with central values being  $1.04\sigma$  ( $0.80\sigma$ ) lower than  $w_X = -1$ ; and for flat (non-flat)  $\phi$ CDM,  $\alpha < 6.756$  ( $\alpha < 7.239$ ), with  $\alpha = 0$  being within  $1\sigma$ .

<sup>12</sup> We note that cosmological parameter constraints from Platinum, A101, and Platinum + A101 data are also consistent with those from QSO-AS, H II G, and Mg II QSO data, so we also investigate the joint QSO-AS + H II G + Mg II QSO + Platinum + A101 (QHPMAP101) data combination. As seen in Tables 4 and 5, we find no significant differences between the QHPMAP101 cosmological constraints and those from the QSO-AS + H II G + Mg II QSO + A118 data combination that contains fewer non-cosmological parameters.

<sup>11</sup> We use PYTHON package GETDIST (Lewis 2019) to analyze the samples and generate the plots.

### 5.3 Constraints from $H(z) + \text{BAO} + \text{SN} + \text{QSO-AS} + \text{H II}G + \text{Mg II QSO} + \text{A118}$ (HzBSNQHMA) data

Cosmological parameter constraints from  $H(z) + \text{BAO} + \text{SN}$  data are consistent with those from QSO-AS + H II $G$  + Mg II QSO + A118 data. From model to model, there are differences, ranging from  $-0.41\sigma$  (flat XCDM) to  $1.45\sigma$  (flat  $\phi$ CDM), between  $\Omega_{m0}$  constraints from  $H(z) + \text{BAO} + \text{SN}$  data and those from QSO-AS + H II $G$  + Mg II QSO + A118 data; and there are differences, ranging from  $0.73\sigma$  (non-flat  $\phi$ CDM) to  $1.48\sigma$  (flat XCDM), between  $H_0$  constraints from QSO-AS + H II $G$  + Mg II QSO + A118 data and those from  $H(z) + \text{BAO} + \text{SN}$  data. For the XCDM parametrizations,  $H(z) + \text{BAO} + \text{SN}$  data slightly prefer non-phantom dark energy dynamics, whereas QSO-AS + H II $G$  + Mg II QSO + A118 data prefer phantom dark energy dynamics, however, their differences are within  $1\sigma$ . As can be seen in the (d) panels of Figs. 1–6, the two-dimensional posterior cosmological constraints from  $H(z) + \text{BAO} + \text{SN}$  data and QSO-AS + H II $G$  + Mg II QSO + A118 data are significantly more mutually consistent than the less than  $1.5\sigma$  differences between the maximum and minimum one-dimensional posterior mean values discussed above. Consequently we can combine these data in a joint HzBSNQHMA data analysis; we discuss the results from this analysis next.

The constraints from HzBSNQHMA data on  $\Omega_{m0}$  range from a low of  $0.286 \pm 0.015$  (flat  $\phi$ CDM) to a high of  $0.300 \pm 0.012$  (flat  $\Lambda$ CDM), with a difference of  $0.73\sigma$ .

The  $H_0$  constraints range from a low of  $69.50 \pm 1.14$  km s $^{-1}$  Mpc $^{-1}$  (flat  $\phi$ CDM) to a high of  $69.87 \pm 1.13$  km s $^{-1}$  Mpc $^{-1}$  (flat  $\Lambda$ CDM), with a difference of  $0.23\sigma$ , which are  $0.50\sigma$  (flat  $\phi$ CDM) and  $0.62\sigma$  (flat  $\Lambda$ CDM) higher than the median statistics estimate of  $H_0 = 68 \pm 2.8$  km s $^{-1}$  Mpc $^{-1}$  (Chen & Ratra 2011), and  $2.14\sigma$  (flat  $\phi$ CDM) and  $1.93\sigma$  (flat  $\Lambda$ CDM) lower than the local Hubble constant measurement of  $H_0 = 73.2 \pm 1.3$  km s $^{-1}$  Mpc $^{-1}$  (Riess et al. 2021).<sup>13</sup>

The constraints on  $\Omega_{k0}$  are  $0.018 \pm 0.059$ ,  $-0.009^{+0.077}_{-0.083}$ , and  $-0.040^{+0.064}_{-0.072}$  for non-flat  $\Lambda$ CDM, XCDM, and  $\phi$ CDM, respectively. Following the same pattern as  $H(z) + \text{BAO} + \text{SN}$  data results, flat hypersurfaces are also well within  $1\sigma$ .

There is a slight preference for dark energy dynamics. For flat (non-flat) XCDM,  $w_X = -0.959 \pm 0.059$  ( $w_X = -0.959^{+0.090}_{-0.063}$ ), with central values being  $0.69\sigma$  ( $0.65\sigma$ ) higher than  $w_X = -1$ ; and for flat (non-flat)  $\phi$ CDM,  $\alpha = 0.249^{+0.069}_{-0.239}$  ( $\alpha = 0.316^{+0.101}_{-0.292}$ ), with central values being  $1.04\sigma$  ( $1.08\sigma$ ) away from  $\alpha = 0$ .

<sup>13</sup> Other local determinations of  $H_0$  result in somewhat lower central values with somewhat larger error bars (Rigault et al. 2015; Zhang et al. 2017; Dhawan et al. 2018; Fernández Arenas et al. 2018; Breuval et al. 2020; Efstathiou 2020; Khetan et al. 2021; Rameez & Sarkar 2021; Freedman 2021). Our  $H_0$  determinations here are consistent with earlier median statistics estimates (Gott et al. 2001; Calabrese et al. 2012) and with other recent  $H_0$  determinations (Chen et al. 2017; DES Collaboration 2018; Gómez-Valet & Amendola 2018; Planck Collaboration 2020; Domínguez et al. 2019; Cuceu et al. 2019; Zeng & Yan 2019; Schöneberg et al. 2019; Blum et al. 2020; Lyu et al. 2020; Philcox et al. 2020; Birrer et al. 2020; Denzel et al. 2021; Pogosian et al. 2020; Kim et al. 2020; Harvey 2020; Boruah et al. 2021; Zhang & Huang 2021; Lin & Ishak 2021; Wu et al. 2022).

### 5.4 Model Comparison

From the AIC, BIC, and DIC values listed in Table 4, we find the following results:

1) **AIC**  $H(z) + \text{BAO}$  data favor flat  $\phi$ CDM the most, Mg II QSO + A118 data favor flat XCDM the most, QSO-AS + H II $G$  data favor non-flat XCDM the most, and the other data combinations favor flat  $\Lambda$ CDM the most. However the evidence against the rest of the models/parametrizations is either only weak or positive.

2) **BIC** All data combinations favor flat  $\Lambda$ CDM the most.  $H(z) + \text{BAO}$  data only provide weak or positive evidence against other models/parametrizations.

Both Mg II QSO + A118 and QSO-AS + H II $G$  data provide strong (very strong) evidence against non-flat XCDM (non-flat  $\phi$ CDM) and positive evidence against the others.

QSO-AS + H II $G$  + Mg II QSO + A118 data provide strong (very strong) evidence against flat  $\phi$ CDM (non-flat XCDM and non-flat  $\phi$ CDM) and positive evidence against non-flat  $\Lambda$ CDM and flat XCDM.

$H(z) + \text{BAO} + \text{SN}$  data provide strong (very strong) evidence against non-flat  $\Lambda$ CDM (non-flat XCDM and non-flat  $\phi$ CDM) and positive evidence against flat XCDM and flat  $\phi$ CDM.

$H(z) + \text{BAO} + \text{SN} + \text{QSO-AS} + \text{H II}G + \text{Mg II QSO} + \text{A118}$  data provide very strong evidence against non-flat XCDM and non-flat  $\phi$ CDM, and strong evidence against the others.

QSO-AS + H II $G$  + Mg II QSO + Platinum + A101 data provide strong (very strong) evidence against flat  $\phi$ CDM (non-flat XCDM and non-flat  $\phi$ CDM) and positive evidence against non-flat  $\Lambda$ CDM and flat XCDM.

3) **DIC**  $H(z) + \text{BAO}$ , Mg II QSO + A118, and  $H(z) + \text{BAO} + \text{SN}$  data favor flat  $\phi$ CDM the most, and the other data combinations favor flat  $\Lambda$ CDM the most. There is strong evidence against non-flat XCDM from QSO-AS + H II $G$  data, strong evidence against non-flat  $\phi$ CDM from QSO-AS + H II $G$ , QSO-AS + H II $G$  + Mg II QSO + A118, and QSO-AS + H II $G$  + Mg II QSO + Platinum + A101 data, and weak or positive evidence against the others from the remaining data sets.

Perhaps the most reliable summary conclusion is that, based on DIC, the  $H(z) + \text{BAO} + \text{SN} + \text{QSO-AS} + \text{H II}G + \text{Mg II QSO} + \text{A118}$  data combination does not provide strong evidence against any of the cosmological models/parametrizations.

## 6 CONCLUSION

In this paper we use many of the most up-to-date available non-CMB data sets to determine cosmological constraints. We analyze 32  $H(z)$ , 12 BAO, 1048 Pantheon SN Ia, 20 binned DES-3yr SN Ia, 120 QSO-AS, 181 H II $G$ , 78 Mg II QSO, 118 (101) A118 (A101) GRB, and 50 Platinum GRB measurements and find that the cosmological constraints from each data set are mutually consistent. We find very small differences between cosmological constraints determined from QSO-AS + H II $G$  + Mg II QSO + A118 data and those from QSO-AS + H II $G$  + Mg II QSO + Platinum + A101 data, so report only the cosmological constraints

from joint  $H(z) + \text{BAO} + \text{SN} + \text{QSO-AS} + \text{H II G} + \text{Mg II QSO} + \text{A118}$  (HzBSNQHMA) data.

The HzBSNQHMA data provide a fairly restrictive summary value<sup>14</sup> of  $\Omega_{m0} = 0.295 \pm 0.017$  that agrees well with many other recent measurements and a fairly restrictive summary value of  $H_0 = 69.7 \pm 1.2 \text{ km s}^{-1} \text{ Mpc}^{-1}$  that is in better agreement with the result of Chen & Ratra (2011) than with the result of Riess et al. (2021).<sup>15</sup> Our  $H_0$  measurement here lies in the middle of the flat  $\Lambda\text{CDM}$  model result of Planck Collaboration (2020) and the local expansion rate result of Riess et al. (2021), slightly closer to the former. Based on DIC, the HzBSNQHMA data compilation prefers flat  $\Lambda\text{CDM}$  the most, but does not rule out mild dark energy dynamics or a little spatial curvature energy density (evidence against them is either weak or positive).

We hope that in the near future the quality and amount of the types of lower-redshift, non-CMB, data we have used here will improve enough to result in cosmological parameter error bars comparable to those from *Planck* CMB anisotropy data.

## ACKNOWLEDGEMENTS

We thank Javier de Cruz Pérez and Chan-Gyung Park for useful discussions about BAO data. This research was supported in part by DOE grant DE-SC0011840. The computations for this project were performed on the Beocat Research Cluster at Kansas State University, which is funded in part by NSF grants CNS-1006860, EPS-1006860, EPS-0919443, ACI-1440548, CHE-1726332, and NIH P20GM113109.

## DATA AVAILABILITY

The H II G data were provided to us by the authors of González-Morán et al. (2021) and will be shared on request to the corresponding author with the permission of the authors of González-Morán et al. (2021). All other data we use are publicly available in the papers cited in Sec. 3.

## REFERENCES

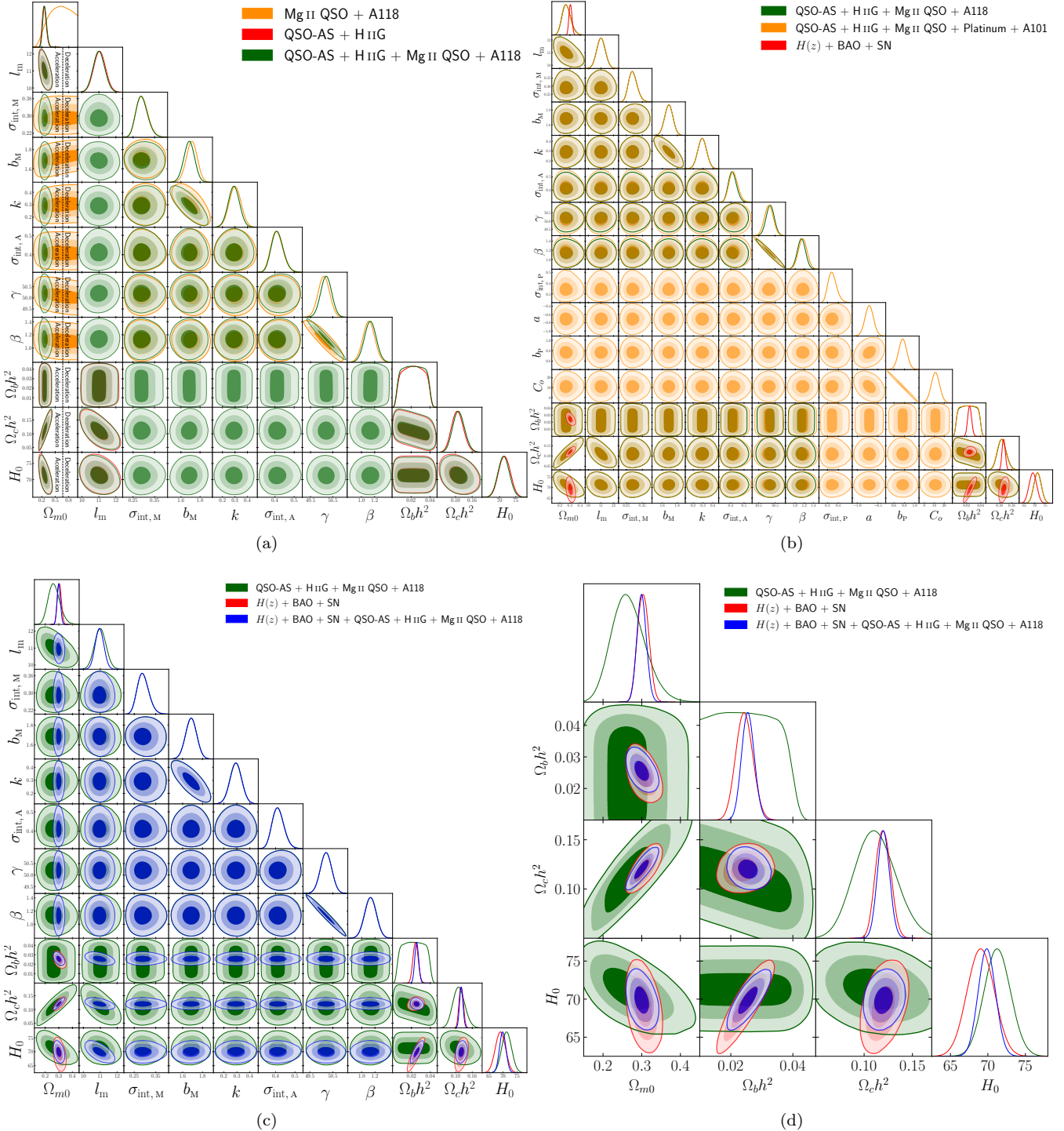
- Abdalla E., et al., 2022, preprint, ([arXiv:2203.06142](#))
- Amati L., D'Agostino R., Luongo O., Muccino M., Tantalo M., 2019, *MNRAS*, **486**, L46
- Arjona R., Nesseris S., 2021, *Phys. Rev. D*, **103**, 103539
- Audren B., Lesgourgues J., Benabed K., Prunet S., 2013, *J. Cosmology Astropart. Phys.*, **2013**, 001
- <sup>14</sup> As in Cao et al. (2021b, 2022b), the summary central value is computed from the mean of the two central-most of the six mean values and the summary uncertainty is computed from the quadrature sum of the systematic uncertainty, defined to be half of the difference between the two central-most mean values, and the statistical uncertainty, defined to be the average of the error bars of the two central-most results.
- <sup>15</sup> Our model-independent  $H_0$  error bar is slightly smaller than that of Riess et al. (2021) and is a factor of 2.2 larger than that of the flat  $\Lambda\text{CDM}$  model (Planck Collaboration 2020) TT,TE,EE+lowE+lensing CMB anisotropy  $H_0$  error bar while our  $\Omega_{m0}$  error bar is a factor of 2.3 larger than the corresponding *Planck* flat  $\Lambda\text{CDM}$  one.
- Bautista J. E., et al., 2021, *MNRAS*, **500**, 736
- Birrer S., et al., 2020, *A&A*, **643**, A165
- Blas D., Lesgourgues J., Tram T., 2011, *J. Cosmology Astropart. Phys.*, **2011**, 034
- Blum K., Castorina E., Simonović M., 2020, *ApJ*, **892**, L27
- Borghi N., Moresco M., Cimatti A., 2022, *ApJ*, **928**, L4
- Boruah S. S., Hudson M. J., Lavaux G., 2021, *MNRAS*, **507**, 2697
- Breuval L., et al., 2020, *A&A*, **643**, A115
- Calabrese E., Archidiacono M., Melchiorri A., Ratra B., 2012, *Phys. Rev. D*, **86**, 043520
- Cao S., Zheng X., Biesiada M., Qi J., Chen Y., Zhu Z.-H., 2017, *A&A*, **606**, A15
- Cao S., Ryan J., Ratra B., 2020, *MNRAS*, **497**, 3191
- Cao S., Ryan J., Khadka N., Ratra B., 2021a, *MNRAS*, **501**, 1520
- Cao S., Ryan J., Ratra B., 2021b, *MNRAS*, **504**, 300
- Cao S., Dainotti M., Ratra B., 2022a, preprint, ([arXiv:2204.08710](#))
- Cao S., Ryan J., Ratra B., 2022b, *MNRAS*, **509**, 4745
- Cao S., Khadka N., Ratra B., 2022c, *MNRAS*, **510**, 2928
- Cao S., Dainotti M., Ratra B., 2022d, *MNRAS*, **512**, 439
- Carter P., Beutler F., Percival W. J., Blake C., Koda J., Ross A. J., 2018, *MNRAS*, **481**, 2371
- Chávez R., Terlevich R., Terlevich E., Bresolin F., Melnick J., Plionis M., Basilakos S., 2014, *MNRAS*, **442**, 3565
- Chen G., Ratra B., 2011, *PASP*, **123**, 1127
- Chen Y., Ratra B., Biesiada M., Li S., Zhu Z.-H., 2016, *ApJ*, **829**, 61
- Chen Y., Kumar S., Ratra B., 2017, *ApJ*, **835**, 86
- Cuceu A., Farr J., Lemos P., Font-Ribera A., 2019, *J. Cosmology Astropart. Phys.*, **2019**, 044
- Czerny B., et al., 2021, *Acta Physica Polonica A*, **139**, 389
- DES Collaboration 2018, *MNRAS*, **480**, 3879
- DES Collaboration 2019a, *Phys. Rev. D*, **99**, 123505
- DES Collaboration 2019b, *MNRAS*, **483**, 4866
- DES Collaboration 2019c, *ApJ*, **874**, 150
- Dai Y., Zheng X.-G., Li Z.-X., Gao H., Zhu Z.-H., 2021, *A&A*, **651**, L8
- Dainotti M. G., Postnikov S., Hernandez X., Ostrowski M., 2016, *ApJ*, **825**, L20
- Dainotti M. G., Nagataki S., Maeda K., Postnikov S., Pian E., 2017, *A&A*, **600**, A98
- Dainotti M. G., Lenart A. Ł., Sarracino G., Nagataki S., Capozziello S., Fraija N., 2020, *ApJ*, **904**, 97
- Dainotti M. G., Nielson V., Sarracino G., Rinaldi E., Nagataki S., Capozziello S., Gnedin O. Y., Bargiacchi G., 2022b, preprint, ([arXiv:2203.15538](#))
- Dainotti M. G., Bardiacchi G., Lukasz Lenart A., Capozziello S., Colgain E. O., Solomon R., Stojkovic D., Sheikh-Jabbari M. M., 2022a, preprint, ([arXiv:2203.12914](#))
- de Cruz Perez J., Sola Peracaula J., Gomez-Valent A., Moreno-Pulido C., 2021, preprint, ([arXiv:2110.07569](#))
- Demianski M., Piedipalumbo E., Sawant D., Amati L., 2021, *MNRAS*, **506**, 903
- Denzel P., Coles J. P., Saha P., Williams L. L. R., 2021, *MNRAS*, **501**, 784
- Dhawan S., Jha S. W., Leibundgut B., 2018, *A&A*, **609**, A72
- Dhawan S., Alsing J., Vagnozzi S., 2021, *MNRAS*, **506**, L1
- Di Valentino E., et al., 2021a, *Classical and Quantum Gravity*, **38**, 153001
- Di Valentino E., Melchiorri A., Silk J., 2021b, *ApJ*, **908**, L9
- Domínguez A., et al., 2019, *ApJ*, **885**, 137
- du Mas des Bourboux H., et al., 2020, *ApJ*, **901**, 153
- eBOSS Collaboration 2021, *Phys. Rev. D*, **103**, 083533
- Efstathiou G., 2020, preprint, ([arXiv:2007.10716](#))
- Efstathiou G., Gratton S., 2020, *MNRAS*, **496**, L91
- Fana Dirirsa F., et al., 2019, *ApJ*, **887**, 13
- Farooq O., Ranjeet Madiyar F., Crandall S., Ratra B., 2017, *ApJ*, **835**, 26

Table 4: Unmarginalized best-fitting parameter values for all models from various combinations of data.

Model	Data set	$\Omega_bh^2$	$\Omega_ch^2$	$\Omega_{k0}$	$\Omega_{\text{m}0}$	$w_{\text{IX}}/\alpha^{\text{a}}$	$H_0^{\text{b}}$	$\sigma_{\text{int}, \text{M}}$	$b_{\text{m}}$	$k$	$\sigma_{\text{int}, \text{A}}$	$\gamma$	$\beta$	$\sigma_{\text{int}, \text{P}}$	$a$	$b_p$	$C_o$	$-2\ln\mathcal{L}_{\text{max}}$	AIC	BIC	DIC	$\Delta\text{AIC}$	$\Delta\text{BIC}$	$\Delta\text{DIC}$	
Flat $\Lambda\text{CDM}$	$H(z) + \text{BAO}$	0.0244	0.1181	0.301	—	—	68.98	—	—	—	—	—	—	—	—	—	—	25.64	31.64	36.99	32.32	0.00	0.00	0.00	
	MgII QSO + A118	—	0.2526	0.567	—	—	0.286	1.711	0.300	0.398	50.12	1.105	—	—	—	—	—	159.64	173.64	196.59	173.37	0.00	0.00	0.00	
	QSO-AS + H <sub>1</sub> G	0.0332	0.0947	0.251	—	—	71.53	11.06	—	—	—	—	—	—	—	—	—	786.45	794.45	809.28	792.69	0.00	0.00	0.00	
	QSO-AS + MgII QSO + A118	0.0183	0.1127	0.258	—	—	71.50	11.04	0.282	1.682	0.294	0.404	50.23	1.124	—	—	—	947.34	967.34	1009.43	966.23	0.00	0.00	0.00	
	$H(z) + \text{BAO} + \text{SN}$	0.0242	0.1191	0.304	—	—	68.86	—	—	—	—	—	—	—	—	—	—	1082.39	1088.39	1103.44	1089.92	0.00	0.00	0.00	
	HzBSNQHMA <sup>c</sup>	0.0238	0.1207	0.300	—	—	70.06	10.93	0.286	1.671	0.296	0.406	50.20	1.110	—	—	—	2631.30	2651.30	2665.13	2651.86	0.00	0.00	0.00	
Non-flat $\Lambda\text{CDM}$	QHMPA10 <sup>e</sup>	0.0197	0.1144	0.264	—	—	71.41	11.02	0.283	1.673	0.315	0.410	50.11	1.169	0.321	-0.746	0.773	10.81	964.62	992.62	1022.44	990.65	0.00	0.00	0.00
	$H(z) + \text{BAO}$	0.0260	0.1098	0.292	0.048	—	68.35	—	—	—	—	—	—	—	—	—	—	25.30	33.30	40.43	33.87	1.66	3.44	1.54	
	MgII QSO + A118	—	0.2692	0.601	0.252	—	72.91	11.60	—	0.281	1.713	0.308	0.401	50.07	1.117	—	—	—	159.65	175.65	201.87	174.46	2.01	5.28	1.09
	QSO-AS + H <sub>1</sub> G	0.0228	0.1145	0.260	-0.360	—	72.25	11.29	0.282	1.678	0.299	0.410	50.27	1.106	—	—	—	784.18	794.18	812.71	793.24	-0.27	3.43	0.55	
	QSO-AS + H <sub>1</sub> G + MgII QSO + A118	0.0261	0.1186	0.278	-0.254	—	68.53	—	—	—	—	—	—	—	—	—	—	945.97	967.97	1014.27	966.91	0.63	4.84	0.69	
	$H(z) + \text{BAO} + \text{SN}$	0.0255	0.1121	0.295	0.035	—	69.90	10.94	0.281	1.674	0.301	0.400	50.20	1.126	—	—	—	1082.11	1090.11	1101.16	1091.17	1.72	6.72	1.24	
Non-flat $\phi\text{CDM}$	HzBSNQHMA <sup>d</sup>	0.0261	0.1182	0.297	0.008	—	71.56	11.37	0.287	1.682	0.304	0.411	50.20	1.132	0.329	-0.674	0.790	9.64	963.83	993.83	1057.92	992.04	1.21	5.48	1.39
	QHMPA10 <sup>e</sup>	0.0246	0.1161	0.276	-0.221	—	71.41	11.37	0.287	1.682	0.304	0.411	50.20	1.132	—	—	—	22.39	30.39	37.52	30.63	-1.25	0.53	-1.69	
	$H(z) + \text{BAO}$	0.0296	0.0951	0.290	—	-0.754	65.79	—	—	—	—	—	—	—	—	—	—	156.84	172.84	199.07	174.36	-0.80	2.48	0.99	
	MgII QSO + A118	—	0.0448	0.143	—	-4.972	—	—	0.279	1.554	0.292	0.407	50.65	1.126	—	—	—	786.05	796.05	814.58	795.03	1.60	5.30	2.34	
	QSO-AS + H <sub>1</sub> G	0.0174	0.1308	0.285	—	-1.280	72.32	11.23	—	—	—	—	—	—	—	—	—	946.23	968.23	1014.52	967.53	0.89	5.09	1.31	
	QSO-AS + H <sub>1</sub> G + MgII QSO + A118	0.0268	0.1155	0.298	—	-1.505	72.94	11.32	0.282	1.679	0.290	0.401	50.24	1.122	—	—	—	1081.34	1089.34	1109.40	1090.43	0.95	5.96	0.50	
Non-flat $\chi\text{CDM}$	$H(z) + \text{BAO} + \text{SN}$	0.0258	0.1115	0.295	—	-0.940	68.37	—	—	—	—	—	—	—	—	—	—	2030.88	2052.88	212.10	2053.30	1.58	6.97	1.44	
	HzBSNQHMA <sup>d</sup>	0.0266	0.1162	0.296	—	-0.975	69.62	10.94	0.280	1.696	0.278	0.406	50.24	1.118	—	—	—	1081.28	1091.28	1116.35	1092.47	2.89	12.91	2.55	
	QHMPA10 <sup>e</sup>	0.0176	0.1450	0.311	—	-1.573	72.46	11.41	0.276	1.686	0.294	0.417	50.12	1.168	0.326	-0.682	0.756	11.45	963.77	993.77	1057.86	992.26	1.15	5.42	1.61
	$H(z) + \text{BAO}$	0.0289	0.0985	0.296	-0.053	-0.730	65.76	—	—	—	—	—	—	—	—	—	—	22.13	32.13	41.05	32.51	0.49	4.06	0.19	
	MgII QSO + A118	—	0.0169	0.086	-0.027	-5.000	—	-0.279	1.473	0.298	0.396	50.91	1.118	—	—	—	156.52	174.52	204.63	177.50	0.88	7.44	4.13		
	QSO-AS + H <sub>1</sub> G	0.0300	0.0931	0.065	-0.560	-0.651	71.87	11.45	—	—	—	—	—	—	—	—	—	781.18	793.18	815.43	799.50	-1.27	6.15	6.90	
Non-flat $\phi\text{CDM}$	QSO-AS + H <sub>1</sub> G + MgII QSO + A118	0.0365	0.1224	0.307	-0.087	-1.278	72.14	11.33	0.292	1.677	0.287	0.398	50.23	1.123	—	—	—	946.08	970.08	1020.59	969.33	2.74	11.16	3.11	
	$H(z) + \text{BAO} + \text{SN}$	0.0255	0.1155	0.310	-0.030	-0.322	68.68	—	—	—	—	—	—	—	—	—	—	2030.78	2054.78	2119.38	2055.42	3.48	14.25	3.56	
	HzBSNQHMA <sup>d</sup>	0.0260	0.1158	0.295	-0.016	-0.947	69.53	10.94	0.288	1.697	0.277	0.409	50.15	1.151	—	—	—	963.91	995.91	1064.28	993.76	3.29	11.84	3.11	
	QHMPA10 <sup>e</sup>	0.0354	0.1154	0.292	-0.048	-1.221	72.03	11.31	0.272	1.680	0.294	0.313	50.06	1.178	0.313	-0.736	0.769	10.98	—	—	—	—	—	—	
	$H(z) + \text{BAO}$	0.0310	0.0900	0.280	—	-1.010	65.89	—	—	—	—	—	—	—	—	—	—	22.31	30.31	37.45	29.90	-1.33	0.46	-2.42	
	MgII QSO + A118	—	0.2760	0.615	—	-0.353	—	-0.279	1.714	0.308	0.403	50.09	1.105	—	—	—	159.69	175.69	201.91	172.93	2.05	5.32	-0.44		
Non-flat $\phi\text{CDM}$	QSO-AS + H <sub>1</sub> G	0.0198	0.1066	0.249	—	0.000	71.42	11.10	—	0.280	1.723	0.303	0.401	50.04	1.115	—	—	—	786.46	796.46	815.00	796.31	2.01	5.72	3.62
	QSO-AS + H <sub>1</sub> G + MgII QSO + A118	0.0338	0.0979	0.251	-0.250	0.000	72.53	11.47	—	—	—	—	—	—	—	—	—	784.61	796.61	818.85	801.32	2.16	9.57	8.63	
	$H(z) + \text{BAO} + \text{SN}$	0.0263	0.1097	0.292	—	0.203	68.39	—	—	—	—	—	—	—	—	—	—	1081.22	1089.22	1109.28	1089.91	0.83	5.84	-0.01	
	HzBSNQHMA <sup>d</sup>	0.0274	0.1116	0.289	—	0.150	69.51	10.97	0.280	1.685	0.292	0.409	50.23	1.121	—	—	—	2030.52	2052.52	211.74	2053.18	1.22	6.61	1.33	
	QHMPA10 <sup>e</sup>	0.0388	0.0884	0.251	—	0.015	71.31	11.13	0.287	1.679	0.293	0.412	50.11	1.168	0.317	-0.664	0.775	10.43	964.97	994.97	1059.07	994.25	2.35	6.63	3.60
	$H(z) + \text{BAO}$	0.0306	0.0920	0.284	-0.058	1.200	65.91	—	—	—	—	—	—	—	—	—	—	22.05	32.05	40.97	31.30	0.41	3.98	-1.02	
Non-flat $\phi\text{CDM}$	MgII QSO + A118	—	0.2233	0.507	0.101	6.181	—	-0.280	1.723	0.303	0.401	50.04	1.115	—	—	—	159.63	177.63	207.13	173.84	3.39	10.54	0.47		
	QSO-AS + H <sub>1</sub> G	0.0338	0.0979	0.251	-0.228	0.015	71.91	11.29	0.288	1.673	0.300	0.412	50.23	1.120	—	—	—	946.09	970.09	1020.59	972.93	2.75	11.16	6.70	
	QSO-AS + H <sub>1</sub> G + MgII QSO + A118	0.0373	0.1290	0.265	-0.228	0.023	72.53	68.56	—	—	—	—	—	—	—	—	—	1081.12	1116.19	1161.27	112.73	12.75	1.35	—	
	$H(z) + \text{BAO} + \text{SN}$	0.0261	0.1119	0.295	-0.023	0.253	68.84	10.91	0.284	1.699	0.279	0.411	50.19	1.132	—	—	—	2030.76	2054.76	2119.36	2055.13	3.46	14.23	3.28	
	HzBSNQHMA <sup>d</sup>	0.0251	0.1207	0.300	-0.056	0.195	69.84	10.91	0.281	1.679	0.293	0.412	50.11	1.168	0.317	-0.703	0.777	10.42	963.77	995.77	1061.14	997.14	3.15	11.70	6.49
	QHMPA10 <sup>e</sup>	0.0370	0.0977	0.260	-0.217	0.066	72.15	11.23	0.274	1.689	0.277	0.408	50.08	1.180	0.335	-0.703	0.777	10.42	963.77	995.77					

Table 5: One-dimensional marginalized posterior mean values and uncertainties ( $\pm 1\sigma$  error bars or  $2\sigma$  limits) of the parameters for all models from various combinations of data.

Model	Data set	$\Omega_b h^2$	$\Omega_m$	$\Omega_{k0}$	$w_X/a^3$	$H_0^b$	$l_{\text{in}}^c$	$b_{\text{in}}$	$k$	$\sigma_{\text{int}, \text{A}}$	$\gamma$	$\beta$	$\sigma_{\text{int}, \text{P}}$	$a$	$b_r$	$C_o$	
Flat	$H(z) + \text{BAO}$	$0.0247 \pm 0.030$	$0.1186^{+0.076}_{-0.083}$	$0.30^{+0.016}_{-0.018}$	—	$60.14 \pm 1.85$	—	—	—	—	—	—	—	—	—	—	
$\Lambda$ CDM	$\text{MgII QSO} + \text{Al18}$	—	—	$0.609^{+0.394}_{-0.410}$	—	—	—	—	—	$0.293^{+0.023}_{-0.020}$	$1.712 \pm 0.056$	$0.301 \pm 0.047$	$0.411^{+0.027}_{-0.033}$	$50.10 \pm 0.25$	$11.12 \pm 0.88$	—	
Flat	$\text{QSO-AS} + \text{HIG}$	$0.0225 \pm 0.013$	$0.1076^{+0.097}_{-0.107}$	$0.257^{+0.020}_{-0.022}$	—	—	$7.52 \pm 1.79$	$11.04 \pm 0.34$	—	—	—	—	—	—	—	—	
$\Lambda$ CDM	$\text{QSO-AS} + \text{HIG} + \text{MgII QSO} + \text{Al18}$	$0.0224 \pm 0.016$	$0.1118^{+0.097}_{-0.107}$	$0.246^{+0.020}_{-0.022}$	—	—	$7.28 \pm 1.73$	$11.00 \pm 0.33$	$0.292^{+0.023}_{-0.029}$	$1.688 \pm 0.055$	$0.291 \pm 0.044$	$0.414^{+0.027}_{-0.033}$	$50.20 \pm 0.24$	$1.135 \pm 0.87$	—		
Flat	$H(z) + \text{BAO} + \text{SN}$	$0.0244 \pm 0.027$	$0.1190 \pm 0.076$	$0.304^{+0.014}_{-0.015}$	—	—	$60.04 \pm 1.77$	—	—	—	—	—	—	—	—	—	
$\Lambda$ CDM	$\text{H2SNOHMA}^d$	$0.0256 \pm 0.020$	$0.1201 \pm 0.012$	$0.264^{+0.016}_{-0.017}$	—	—	$60.87 \pm 1.13$	$10.96 \pm 0.25$	$0.292^{+0.023}_{-0.029}$	$1.684 \pm 0.055$	$0.293 \pm 0.044$	$0.413^{+0.026}_{-0.033}$	$50.20 \pm 0.24$	$1.131 \pm 0.87$	—		
Flat	$\text{QHAPAI01}^e$	$0.0225^{+0.018}_{-0.018}$	$0.1105^{+0.017}_{-0.023}$	$0.264^{+0.016}_{-0.017}$	—	—	$71.34^{+1.73}_{-1.74}$	$11.02 \pm 0.34$	$0.291^{+0.023}_{-0.029}$	$1.686 \pm 0.055$	$0.291 \pm 0.044$	$0.421^{+0.026}_{-0.036}$	$50.12 \pm 0.26$	$1.164 \pm 0.94$	$0.346^{+0.032}_{-0.045}$	$-0.710 \pm 0.101$	
Non-flat	$H(z) + \text{BAO}$	$0.0266^{+0.039}_{-0.045}$	$0.1088 \pm 0.0166$	$0.291 \pm 0.023$	—	$68.37 \pm 2.10$	—	—	—	—	—	—	—	—	—	—	
Non-flat	$\text{MgII QSO} + \text{Al18}$	$0.0224 \pm 0.023$	$0.1129^{+0.0218}_{-0.0218}$	$0.260^{+0.039}_{-0.045}$	$0.196^{+0.12}_{-0.25}$	—	$> 27.4$	$0.21^{+1.512}_{-0.872}$	—	$0.294^{+0.023}_{-0.030}$	$1.730^{+0.058}_{-0.053}$	$0.302 \pm 0.047$	$0.411^{+0.027}_{-0.033}$	$50.03 \pm 0.26$	$11.18 \pm 0.89$	—	
Non-flat	$\text{QSO-AS} + \text{HIG}$	$0.0224 \pm 0.0111$	$0.1129^{+0.0223}_{-0.0218}$	$0.271^{+0.039}_{-0.045}$	$0.139^{+0.16}_{-0.28}$	—	$72.25 \pm 1.99$	$11.35 \pm 0.49$	—	$0.291^{+0.023}_{-0.030}$	$1.680 \pm 0.055$	$0.292 \pm 0.044$	$0.415^{+0.027}_{-0.033}$	$50.23 \pm 0.24$	$1.122 \pm 0.88$	—	
Non-flat	$\text{QSO-AS} + \text{HigII QSO} + \text{Al18}$	$0.0225 \pm 0.016$	$0.1162 \pm 0.0218$	$0.271^{+0.045}_{-0.045}$	$0.140^{+0.022}_{-0.070}$	—	$71.77 \pm 1.87$	$11.19 \pm 0.42$	$0.291^{+0.022}_{-0.029}$	$1.675 \pm 0.056$	$0.294 \pm 0.044$	$0.413^{+0.027}_{-0.033}$	$50.20 \pm 0.24$	$1.131 \pm 0.86$	—		
Non-flat	$H(z) + \text{BAO} + \text{SN}$	$0.0260^{+0.037}_{-0.033}$	$0.1119 \pm 0.0157$	$0.294 \pm 0.022$	$0.140^{+0.022}_{-0.022}$	—	$68.62 \pm 1.90$	—	—	—	—	—	—	—	—	—	
Non-flat	$\text{H2SNOHMA}^d$	$0.0265^{+0.033}_{-0.032}$	$0.1168 \pm 0.0127$	$0.295 \pm 0.019$	$0.108 \pm 0.059$	—	$69.79 \pm 1.14$	$10.96 \pm 0.25$	$0.292^{+0.023}_{-0.029}$	$1.685 \pm 0.055$	$0.293 \pm 0.044$	$0.413^{+0.027}_{-0.033}$	$50.20 \pm 0.24$	$1.131 \pm 0.86$	$0.346^{+0.032}_{-0.045}$	$-0.712 \pm 0.102$	
Non-flat	$\text{QHAPAI01}^e$	$0.0224 \pm 0.017$	$0.1138^{+0.0226}_{-0.0216}$	$0.267^{+0.039}_{-0.036}$	$0.096^{+0.127}_{-0.351}$	—	$71.65^{+1.86}_{-1.85}$	$11.15 \pm 0.42$	$0.291^{+0.023}_{-0.029}$	$1.682 \pm 0.055$	$0.292 \pm 0.044$	$0.424^{+0.036}_{-0.036}$	$50.14 \pm 0.26$	$1.155 \pm 0.95$	$0.346^{+0.032}_{-0.045}$	$1.137 \pm 4.34$	
Flat	$H(z) + \text{BAO}$	$0.0295^{+0.042}_{-0.050}$	$0.0969^{+0.0178}_{-0.0152}$	$0.289 \pm 0.020$	—	$-0.734^{+0.140}_{-0.107}$	$66.22^{+2.31}_{-2.34}$	—	—	—	—	—	—	—	—	—	
Flat	$\text{MgII QSO} + \text{Al18}$	—	—	$0.483^{+0.339}_{-0.333}$	—	$< -0.218$	—	—	—	$0.291^{+0.023}_{-0.030}$	$1.670^{+0.055}_{-0.062}$	$0.301 \pm 0.046$	$0.412^{+0.027}_{-0.033}$	$50.25^{+0.28}_{-0.36}$	$1.110 \pm 0.88$	—	
XCDM	$\text{QSO-AS} + \text{HIG}$	$0.0224 \pm 0.0112$	$0.1391^{+0.0233}_{-0.0233}$	$0.305^{+0.036}_{-0.036}$	$0.1449^{+0.055}_{-0.055}$	—	$-1.683^{+0.385}_{-0.385}$	$72.92^{+2.15}_{-2.12}$	$11.31 \pm 0.43$	—	—	—	—	—	—	—	
XCDM	$H(z) + \text{BAO} + \text{SN}$	$0.0262^{+0.033}_{-0.033}$	$0.1120 \pm 0.0110$	$0.295 \pm 0.016$	$0.091 \pm 0.064$	—	$-1.86^{+0.419}_{-0.419}$	$73.14^{+2.14}_{-2.14}$	$11.34 \pm 0.43$	$0.291^{+0.023}_{-0.030}$	$1.675 \pm 0.056$	$0.294 \pm 0.044$	$0.413^{+0.027}_{-0.033}$	$50.24 \pm 0.24$	$1.124 \pm 0.87$	—	
XCDM	$\text{H2SNOHMA}^d$	$0.0271^{+0.037}_{-0.037}$	$0.1449^{+0.0097}_{-0.0097}$	$0.294 \pm 0.015$	$0.055 \pm 0.059$	—	$-0.941 \pm 0.025$	$0.292^{+0.023}_{-0.029}$	$1.685 \pm 0.055$	$0.293 \pm 0.044$	$0.413^{+0.027}_{-0.033}$	$50.20 \pm 0.24$	$1.131 \pm 0.87$	—			
XCDM	$\text{QHAPAI01}^e$	$0.0224 \pm 0.018$	$0.1429^{+0.0248}_{-0.0248}$	$0.310^{+0.044}_{-0.044}$	$-1.801^{+0.121}_{-0.121}$	—	$73.09^{+2.84}_{-2.84}$	$11.33 \pm 0.43$	$0.290^{+0.022}_{-0.029}$	$1.675 \pm 0.056$	$0.294 \pm 0.044$	$0.421^{+0.026}_{-0.036}$	$50.16 \pm 0.26$	$1.152 \pm 0.94$	$0.346^{+0.032}_{-0.045}$	$-0.713 \pm 0.102$	
Flat	$H(z) + \text{BAO}$	$0.0294^{+0.047}_{-0.050}$	$0.0980^{+0.0186}_{-0.0187}$	$0.292 \pm 0.025$	$-0.027 \pm 0.109$	$-0.707^{+0.140}_{-0.108}$	$66.13^{+2.35}_{-2.36}$	—	—	—	—	—	—	—	—	—	
Non-flat	$\text{MgII QSO} + \text{Al18}$	—	—	$> 0.170$	$0.309^{+0.347}_{-0.350}$	$< -0.132$	—	—	$0.293^{+0.023}_{-0.030}$	$1.711^{+0.081}_{-0.088}$	$0.302 \pm 0.047$	$0.413^{+0.027}_{-0.033}$	$50.10^{+0.28}_{-0.32}$	$1.114 \pm 0.91$	—		
Non-flat	$\text{QSO-AS} + \text{HIG}$	$0.0224 \pm 0.0114$	$0.1122^{+0.0326}_{-0.0326}$	$0.288^{+0.086}_{-0.086}$	$0.1379^{+0.345}_{-0.345}$	$-1.670^{+0.463}_{-0.463}$	$72.34^{+2.26}_{-2.26}$	$11.20 \pm 0.49$	$0.291^{+0.023}_{-0.030}$	$1.678 \pm 0.057$	$0.294 \pm 0.045$	$0.414^{+0.027}_{-0.033}$	$50.23 \pm 0.25$	$1.122 \pm 0.89$	—		
XCDM	$\text{QSO-AS} + \text{HigII QSO} + \text{Al18}$	$0.0225 \pm 0.0118$	$0.1327^{+0.0348}_{-0.0348}$	$0.294^{+0.125}_{-0.125}$	$0.054^{+0.227}_{-0.227}$	$-2.042^{+0.451}_{-0.451}$	$72.79^{+2.18}_{-2.18}$	$11.23^{+0.44}_{-0.39}$	$0.291^{+0.023}_{-0.030}$	$1.678 \pm 0.057$	$0.294 \pm 0.045$	$0.414^{+0.027}_{-0.033}$	$50.20 \pm 0.24$	$1.124 \pm 0.87$	—		
XCDM	$H(z) + \text{BAO} + \text{SN}$	$0.0269^{+0.037}_{-0.033}$	$0.1119 \pm 0.0157$	$0.295 \pm 0.022$	$0.001 \pm 0.098$	—	$-0.948^{+0.068}_{-0.068}$	$68.53^{+1.90}_{-1.90}$	—	—	—	—	—	—	—	—	
XCDM	$\text{H2SNOHMA}^d$	$0.0269^{+0.033}_{-0.033}$	$0.1185^{+0.0128}_{-0.0128}$	$0.295 \pm 0.019$	$-0.009^{+0.037}_{-0.037}$	—	$-0.959^{+0.083}_{-0.083}$	$60.95^{+1.16}_{-1.16}$	$10.93 \pm 0.26$	$0.292^{+0.023}_{-0.029}$	$1.685 \pm 0.055$	$0.293 \pm 0.044$	$0.413^{+0.027}_{-0.033}$	$50.20 \pm 0.24$	$1.130 \pm 0.87$	—	
XCDM	$\text{QHAPAI01}^e$	$0.0225 \pm 0.018$	$0.1283^{+0.0230}_{-0.0230}$	$0.286^{+0.062}_{-0.062}$	$0.104^{+0.244}_{-0.244}$	—	$-2.131^{+1.85}_{-1.85}$	$72.10^{+2.43}_{-2.43}$	$11.19 \pm 0.46$	$0.291^{+0.023}_{-0.029}$	$1.673 \pm 0.056$	$0.293 \pm 0.044$	$0.421^{+0.026}_{-0.036}$	$50.14 \pm 0.26$	$1.150 \pm 0.95$	$0.346^{+0.032}_{-0.045}$	$-0.711 \pm 0.102$
Flat	$\text{MgII QSO} + \text{Al18}$	$0.0320^{+0.0414}_{-0.0434}$	$0.0885^{+0.0174}_{-0.0174}$	$0.275 \pm 0.023$	—	$126.47^{+2.22}_{-2.21}$	—	—	$0.293^{+0.023}_{-0.030}$	$1.725 \pm 0.052$	$0.303 \pm 0.046$	$0.411^{+0.026}_{-0.032}$	$50.05 \pm 0.25$	$1.110 \pm 0.87$	—		
Flat	$\text{QSO-AS} + \text{HIG}$	$0.0317^{+0.0401}_{-0.0418}$	$0.0853^{+0.0175}_{-0.0175}$	$0.275 \pm 0.023$	$-0.007 \pm 0.088$	—	$< 6.506$	$70.64 \pm 1.80$	$10.81 \pm 0.34$	$0.293^{+0.023}_{-0.030}$	$1.725 \pm 0.052$	$0.303 \pm 0.046$	$0.411^{+0.026}_{-0.032}$	$50.05 \pm 0.25$	$1.111 \pm 0.89$	—	
$\phi$ CDM	$\text{QSO-AS} + \text{HigII QSO} + \text{Al18}$	$0.0321^{+0.0393}_{-0.0393}$	$0.0857^{+0.0192}_{-0.0192}$	$0.271^{+0.0288}_{-0.0288}$	$0.163^{+0.058}_{-0.058}$	—	$< 6.756$	$70.50 \pm 1.76$	$10.80 \pm 0.34$	$0.292^{+0.023}_{-0.030}$	$1.691 \pm 0.055$	$0.292 \pm 0.045$	$0.415^{+0.028}_{-0.033}$	$50.18 \pm 0.24$	$1.140 \pm 0.88$	—	
$\phi$ CDM	$H(z) + \text{BAO} + \text{SN}$	$0.0278^{+0.0321}_{-0.0321}$	$0.1054^{+0.0117}_{-0.0117}$	$0.287 \pm 0.017$	$-0.005 \pm 0.069$	—	$0.322^{+0.122}_{-0.122}$	$68.20 \pm 1.78$	—	$0.292^{+0.023}_{-0.030}$	$1.686 \pm 0.054$	$0.293 \pm 0.044$	$0.413^{+0.027}_{-0.033}$	$50.20 \pm 0.24$	$1.132 \pm 0.86$	$0.347^{+0.032}_{-0.045}$	$-0.707 \pm 0.102$
$\phi$ CDM	$\text{H2SNOHMA}^d$	$0.0286^{+0.0253}_{-0.0253}$	$0.1089^{+0.0103}_{-0.0103}$	$0.286 \pm 0.015$	—	$0.249^{+0.126}_{-0.126}$	$69.50 \pm 1.14$	$10.92 \pm 0.25$	$0.292^{+0.023}_{-0.030}$	$1.687 \pm 0.055$	$0.291 \pm 0.044$	$0.421^{+0.026}_{-0.036}$	$50.10 \pm 0.26$	$1.172 \pm 0.93$	$0.347^{+0.032}_{-0.045}$	$-0.707 \pm 0.102$	
$\phi$ CDM	$\text{QHAPAI01}^e$	$0.0217^{+0.0164}_{-0.0164}$	$0.0867^{+0.0093}_{-0.0093}$	$0.167^{+0.067}_{-0.067}$	—	$< 7.149$	$70.53 \pm 1.76$	$10.80 \pm 0.34$	$0.292^{+0.023}_{-0.030}$	$1.689 \pm 0.055$	$0.291 \pm 0.044$	$0.421^{+0.026}_{-0.036}$	$50.10 \pm 0.26$	$1.172 \pm 0.93$	$0.347^{+0.032}_{-0.045}$	$-0.7$	



**Figure 1.** One-dimensional likelihood distributions and  $1\sigma$ ,  $2\sigma$ , and  $3\sigma$  two-dimensional likelihood confidence contours for flat  $\Lambda$ CDM from various combinations of data. The zero-acceleration black dashed lines in some (a) panels divide the parameter space into regions associated with currently-accelerating (left) and currently-decelerating (right) cosmological expansion.

- Fernández Arenas D., et al., 2018, *MNRAS*, **474**, 1250  
 Freedman W. L., 2021, *ApJ*, **919**, 16  
 Geng C.-Q., Hsu Y.-T., Lu J.-R., 2022, *ApJ*, **926**, 74  
 Gil-Marín H., et al., 2020, *MNRAS*, **498**, 2492  
 Gómez-Valent A., Amendola L., 2018, *J. Cosmology Astropart. Phys.*, **4**, 051  
 González-Morán A. L., et al., 2019, *MNRAS*, **487**, 4669

- González-Morán A. L., et al., 2021, *MNRAS*, **505**, 1441  
 Gott III J. R., Vogeley M. S., Podariu S., Ratra B., 2001, *ApJ*, **549**, 1  
 Handley W., 2019, *Phys. Rev. D*, **100**, 123517  
 Harvey D., 2020, *MNRAS*, **498**, 2871  
 Hou J., et al., 2021, *MNRAS*, **500**, 1201  
 Hu J. P., Wang F. Y., Dai Z. G., 2021, *MNRAS*, **507**, 730

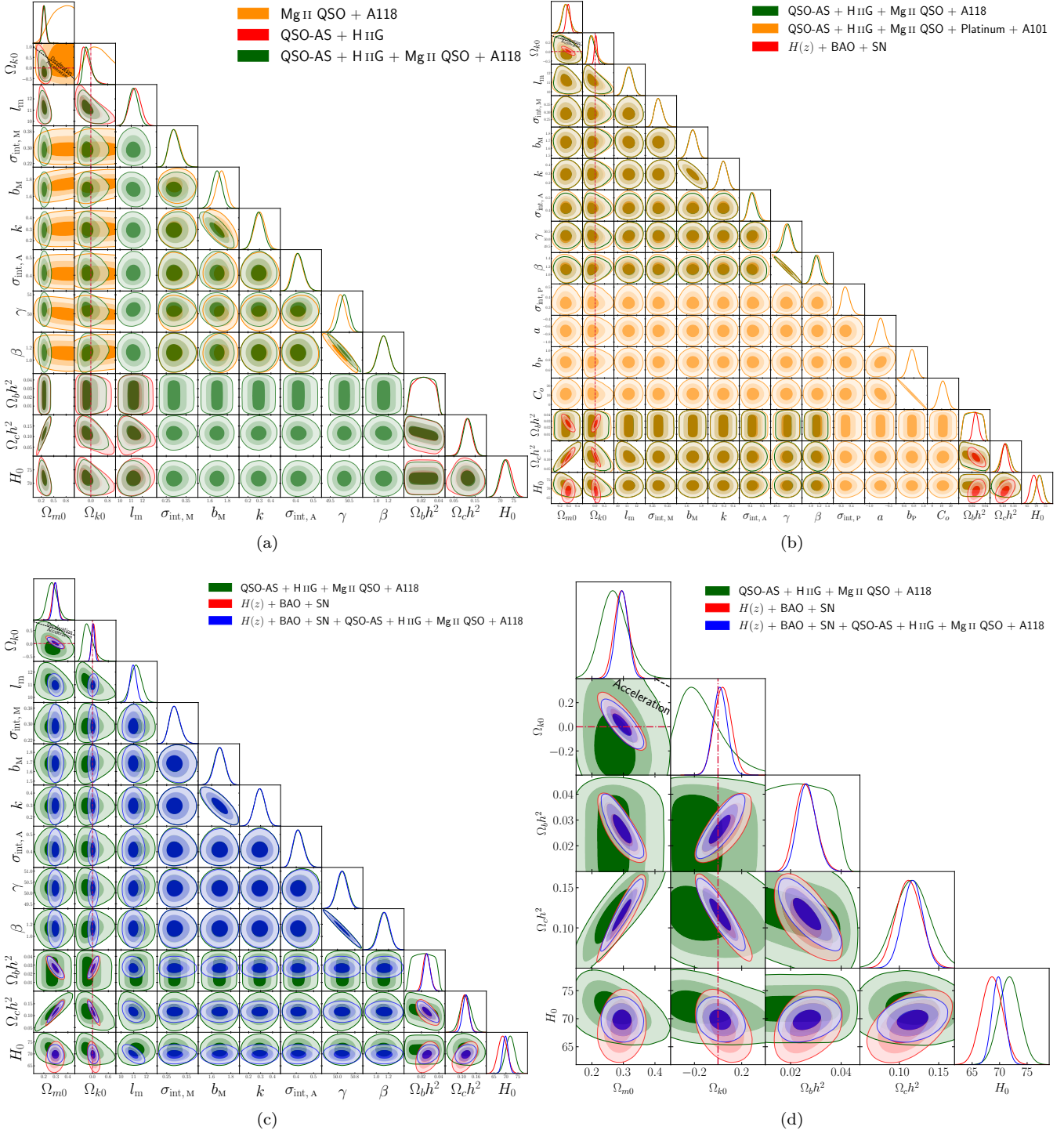


**Figure 2.** Same as Fig. 1 but for non-flat  $\Lambda$ CDM. The zero-acceleration black dashed lines divide the parameter space into regions associated with currently-accelerating (below left) and currently-decelerating (above right) cosmological expansion.

- Jesus J. F., Valentim R., Escobal A. A., Pereira S. H., Benndorf D., 2021, preprint, ([arXiv:2112.09722](https://arxiv.org/abs/2112.09722))  
 Johnson J. P., Sangwan A., Shankaranarayanan S., 2022, *J. Cosmology Astropart. Phys.*, 2022, 024  
 Khadka N., Ratra B., 2020a, *MNRAS*, 492, 4456  
 Khadka N., Ratra B., 2020b, *MNRAS*, 497, 263  
 Khadka N., Ratra B., 2020c, *MNRAS*, 499, 391  
 Khadka N., Ratra B., 2021, *MNRAS*, 502, 6140

- Khadka N., Ratra B., 2022, *MNRAS*, 510, 2753  
 Khadka N., Martínez-Aldama M. L., Zajaček M., Czerny B., Ratra B., 2021a, preprint, ([arXiv:2112.00052](https://arxiv.org/abs/2112.00052))  
 Khadka N., Yu Z., Zajaček M., Martínez-Aldama M. L., Czerny B., Ratra B., 2021b, *MNRAS*, 508, 4722  
 Khadka N., Luongo O., Muccino M., Ratra B., 2021c, *J. Cosmology Astropart. Phys.*, 2021, 042  
 Khetan N., et al., 2021, *A&A*, 647, A72

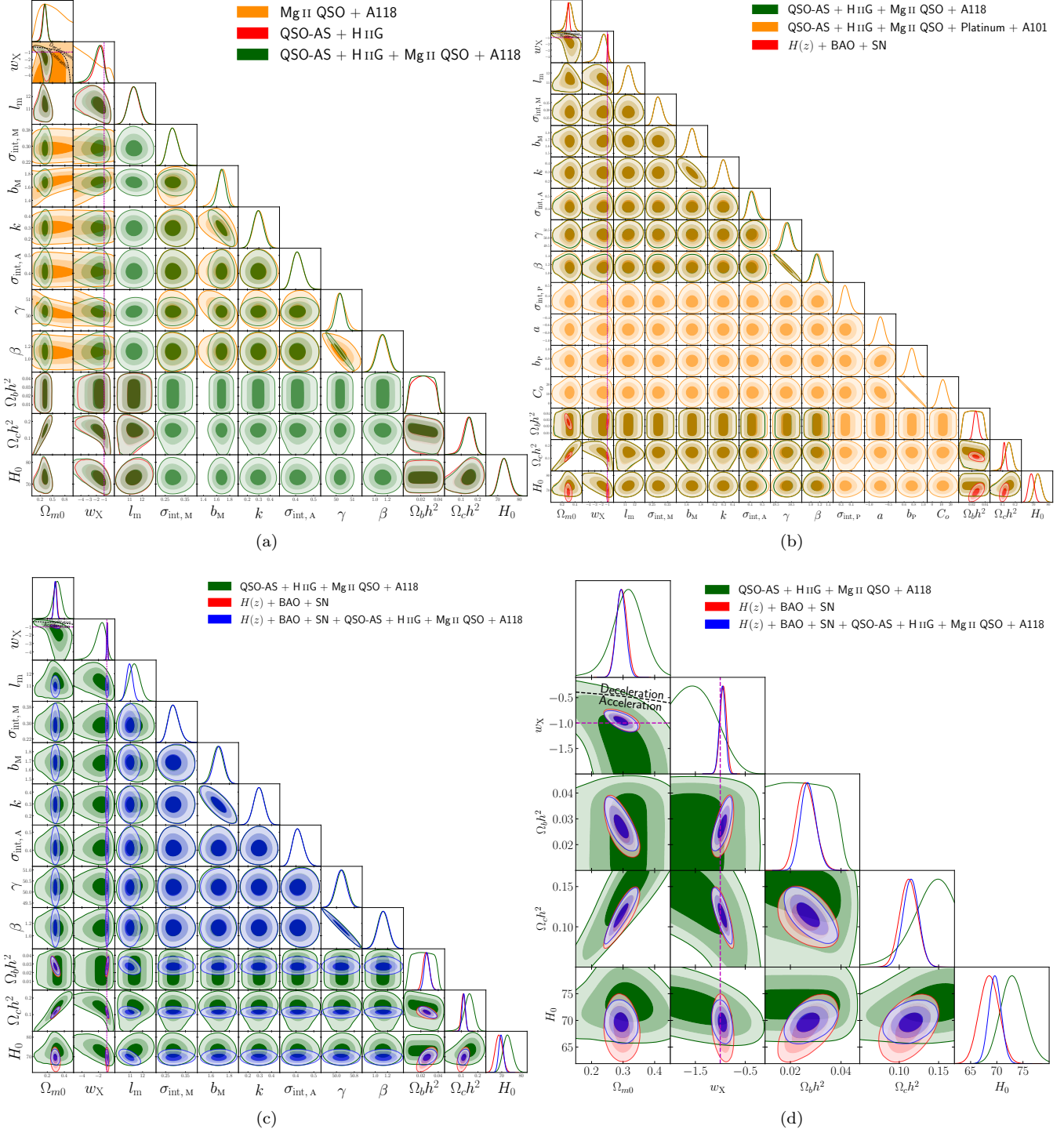


**Figure 3.** One-dimensional likelihood distributions and  $1\sigma$ ,  $2\sigma$ , and  $3\sigma$  two-dimensional likelihood confidence contours for flat XCDM from various combinations of data. The zero-acceleration black dashed lines divide the parameter space into regions associated with currently-accelerating (either below left or below) and currently-decelerating (either above right or above) cosmological expansion. The magenta dashed lines represent  $w_X = -1$ , i.e. flat  $\Lambda$ CDM.

KiDS Collaboration 2021, *A&A*, 649, A88

Kim Y. J., Kang J., Lee M. G., Jang I. S., 2020, *ApJ*, 905, 104

Lewis A., 2019, preprint, ([arXiv:1910.13970](https://arxiv.org/abs/1910.13970))

Li E.-K., Du M., Xu L., 2020, *MNRAS*, 491, 4960

Li X., Keeley R. E., Shafieloo A., Zheng X., Cao S., Biesiada M., Zhu Z.-H., 2021, *MNRAS*, 507, 919

Lian Y., Cao S., Biesiada M., Chen Y., Zhang Y., Guo W., 2021, *MNRAS*, 505, 2111

Lin W., Ishak M., 2021, *J. Cosmology Astropart. Phys.*, 2021, 009

Liu Y., Chen F., Liang N., Yuan Z., Yu H., Wu1 P., 2022, preprint, ([arXiv:2203.03178](https://arxiv.org/abs/2203.03178))

Luongo O., Muccino M., 2021, *Galaxies*, 9, 77

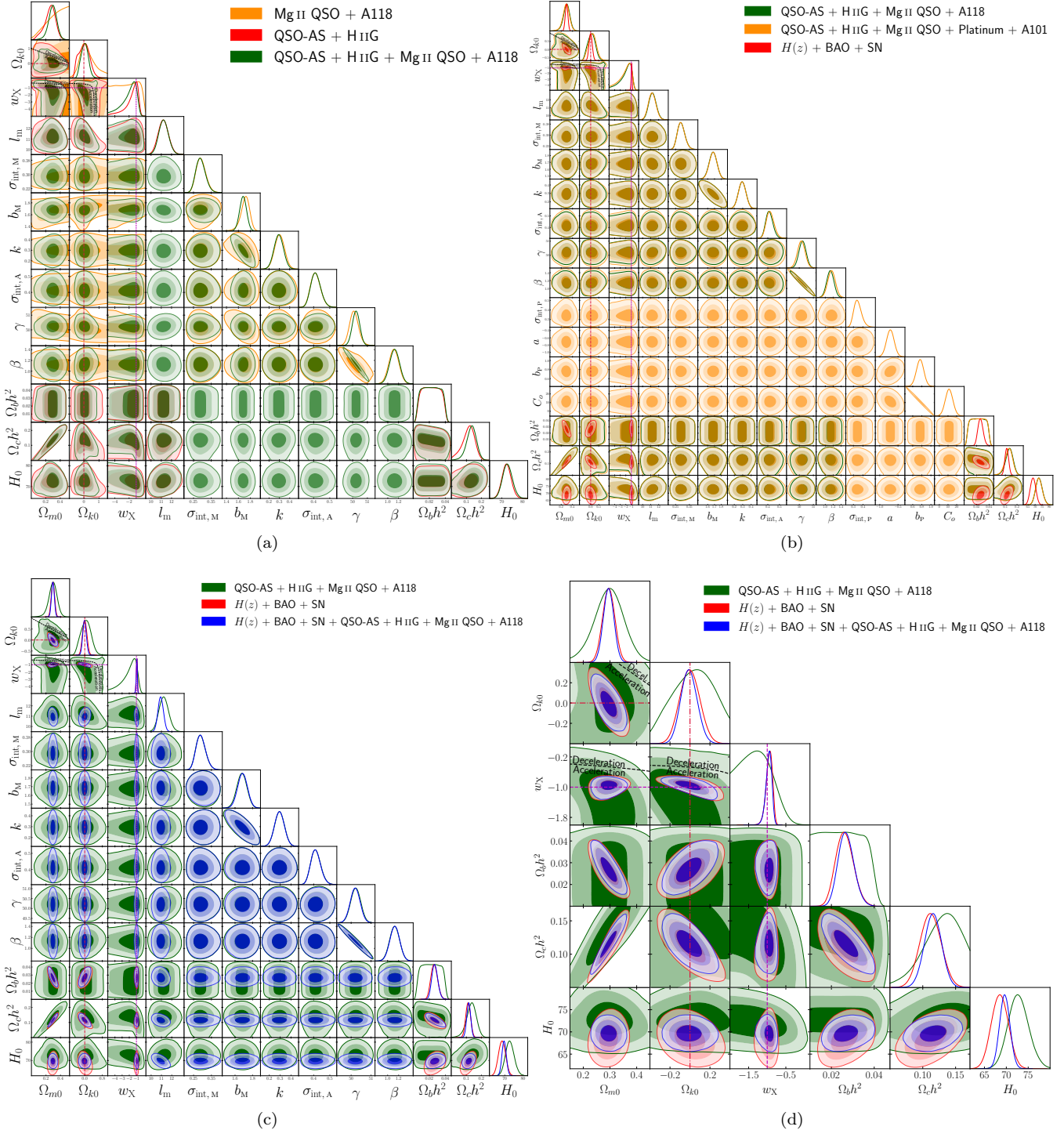


**Figure 4.** Same as Fig. 3 but for non-flat XCDM. The zero-acceleration black dashed lines are computed for the third cosmological parameter set to the  $H(z)$  + BAO data best-fitting values listed in Table 4, and divide the parameter space into regions associated with currently-accelerating (either below left or below) and currently-decelerating (either above right or above) cosmological expansion. The crimson dash-dot lines represent flat hypersurfaces, with closed spatial hypersurfaces either below or to the left. The magenta dashed lines represent  $w_X = -1$ , i.e. non-flat  $\Lambda$ CDM.

- Luongo O., Muccino M., Colgáin E. Ó., Sheikh-Jabbari M. M., Yin L., 2021, preprint, ([arXiv:2108.13228](https://arxiv.org/abs/2108.13228))  
 Lusso E., et al., 2020, *A&A*, 642, A150  
 Lyu M.-Z., Haridasu B. S., Viel M., Xia J.-Q., 2020, *ApJ*, 900, 160

- Mania D., Ratra B., 2012, *Physics Letters B*, 715, 9  
 Mehrabi A., et al., 2022, *MNRAS*, 509, 224  
 Moresco M., 2015, *MNRAS*, 450, L16  
 Moresco M., et al., 2012, *J. Cosmology Astropart. Phys.*, 8, 006  
 Moresco M., et al., 2016, *J. Cosmology Astropart. Phys.*, 5, 014

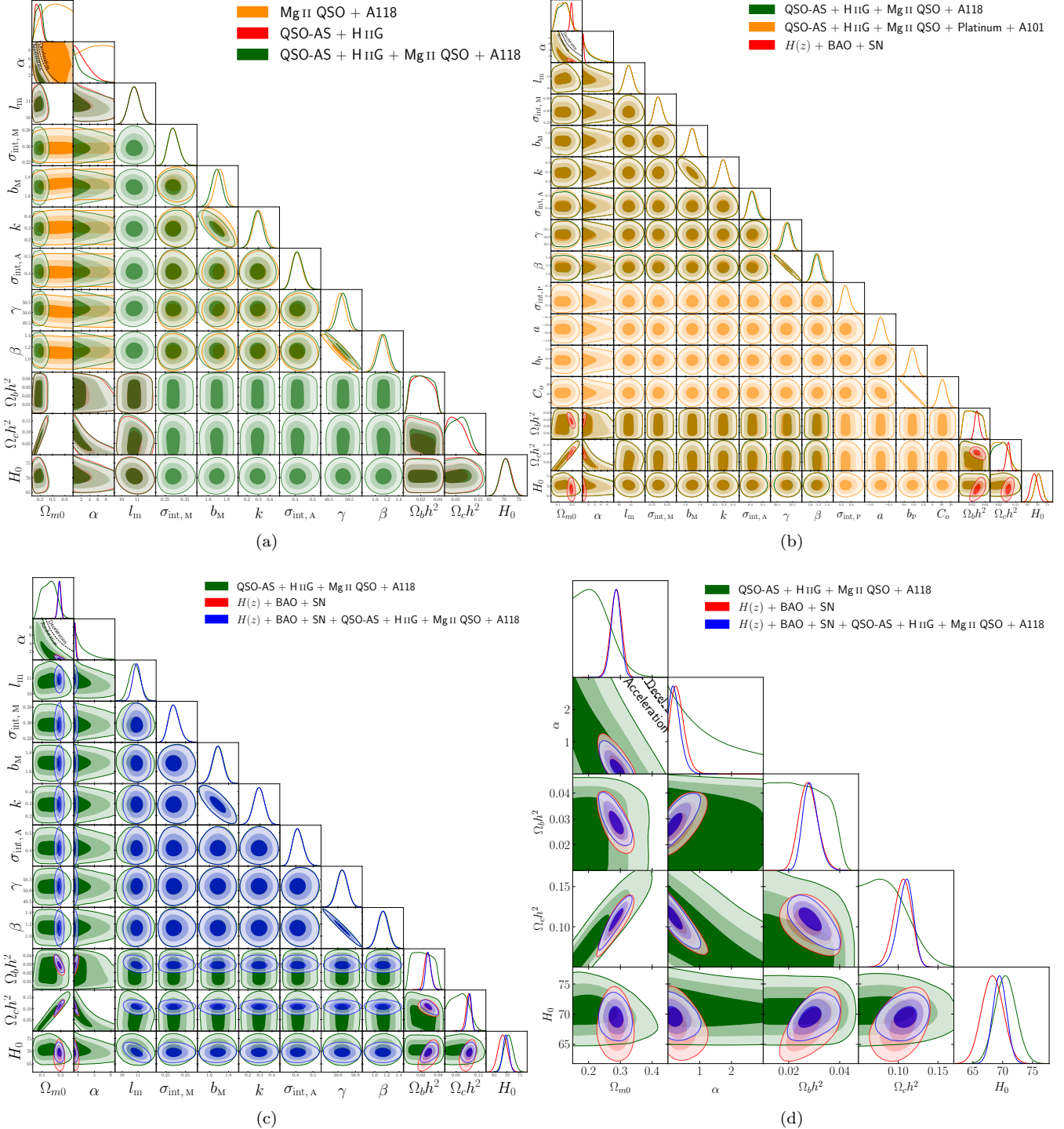


**Figure 5.** One-dimensional likelihood distributions and  $1\sigma$ ,  $2\sigma$ , and  $3\sigma$  two-dimensional likelihood confidence contours for flat  $\phi$ CDM from various combinations of data. The zero-acceleration black dashed lines divide the parameter space into regions associated with currently-accelerating (below left) and currently-decelerating (above right) cosmological expansion. The  $\alpha = 0$  axes correspond to flat  $\Lambda$ CDM.

- Mukherjee P., Banerjee N., 2022, *Phys. Rev. D*, **105**, 063516  
 Neveux R., et al., 2020, *MNRAS*, **499**, 210  
 Ooba J., Ratra B., Sugiyama N., 2018a, *ApJ*, **864**, 80  
 Ooba J., Ratra B., Sugiyama N., 2018b, *ApJ*, **866**, 68  
 Ooba J., Ratra B., Sugiyama N., 2018c, *ApJ*, **869**, 34  
 Ooba J., Ratra B., Sugiyama N., 2019, *Ap&SS*, **364**, 176

- Park C.-G., Ratra B., 2018, *ApJ*, **868**, 83  
 Park C.-G., Ratra B., 2019a, *Ap&SS*, **364**, 82  
 Park C.-G., Ratra B., 2019b, *Ap&SS*, **364**, 134  
 Park C.-G., Ratra B., 2019c, *ApJ*, **882**, 158  
 Park C.-G., Ratra B., 2020, *Phys. Rev. D*, **101**, 083508  
 Pavlov A., Westmoreland S., Saaidi K., Ratra B., 2013, *Phys.*

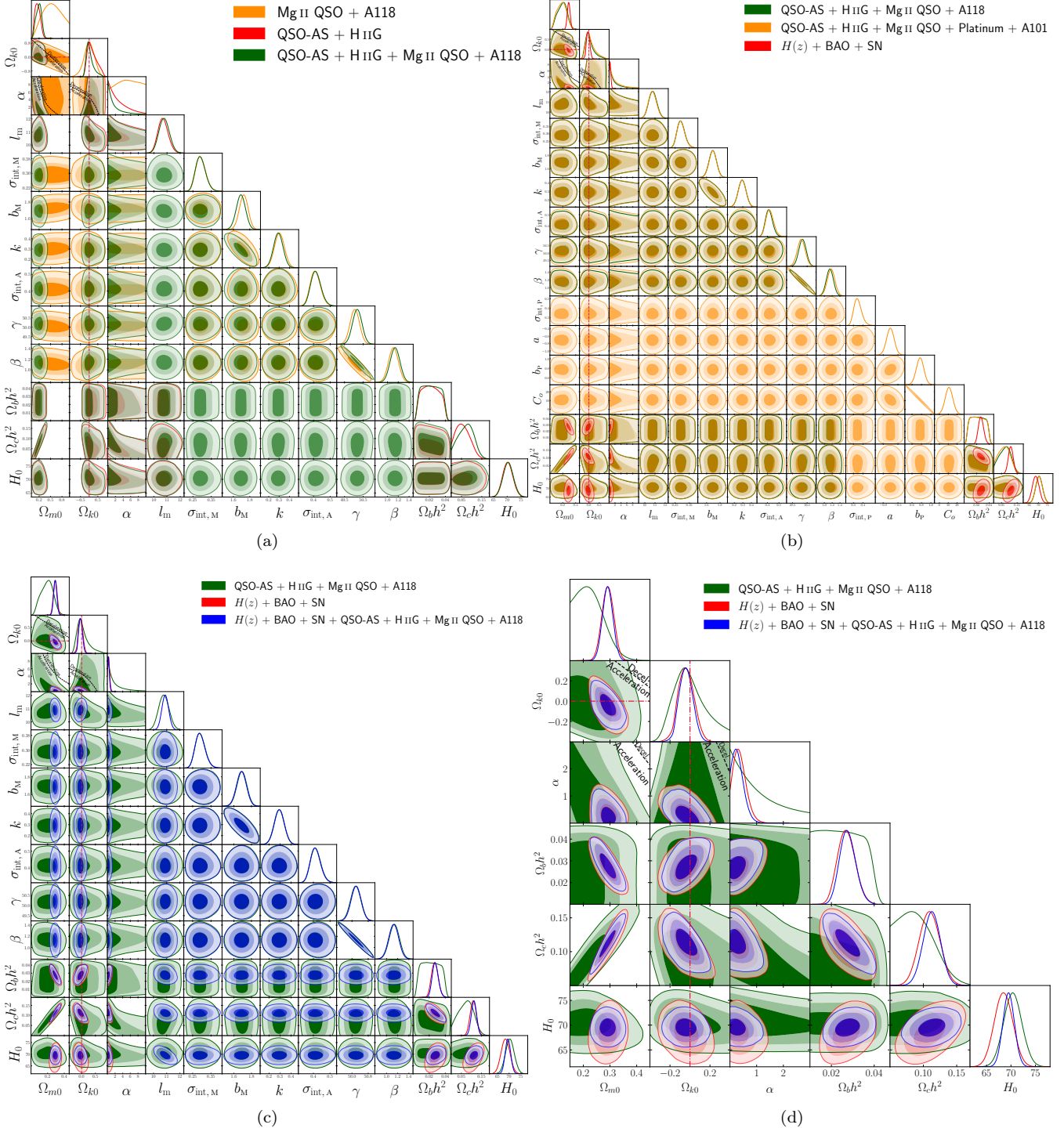


**Figure 6.** Same as Fig. 5 but for non-flat  $\phi$ CDM. The zero-acceleration black dashed lines are computed for the third cosmological parameter set to the  $H(z)$  + BAO data best-fitting values listed in Table 4, and divide the parameter space into regions associated with currently-accelerating (below left) and currently-decelerating (above right) cosmological expansion. The crimson dash-dot lines represent flat hypersurfaces, with closed spatial hypersurfaces either below or to the left. The  $\alpha = 0$  axes correspond to non-flat  $\Lambda$ CDM.

Rev. D, 88, 123513

Peebles P. J. E., 1984, ApJ, 284, 439

Peebles P. J. E., Ratra B., 1988, ApJ, 325, L17

Perivolaropoulos L., Skara F., 2021, preprint, ([arXiv:2105.05208](https://arxiv.org/abs/2105.05208))

Philcox O. H. E., Ivanov M. M., Simonović M., Zaldarriaga M.,

2020, J. Cosmology Astropart. Phys., 2020, 032

Planck Collaboration 2020, A&A, 641, A6

Pogosian L., Zhao G.-B., Jedamzik K., 2020, ApJ, 904, L17

Rameez M., Sarkar S., 2021, Classical and Quantum Gravity, 38, 154005

Rana A., Jain D., Mahajan S., Mukherjee A., 2017, J. Cosmology

- [Astropart. Phys.](#), **2017**, 028
- Ratra B., Peebles P. J. E., 1988, [Phys. Rev. D](#), **37**, 3406
- Ratsimbazafy A. L., Loubser S. I., Crawford S. M., Cress C. M., Bassett B. A., Nichol R. C., Väistönen P., 2017, [MNRAS](#), **467**, 3239
- Renzi F., Hogg N. B., Giarè W., 2022, preprint, ([arXiv:2112.05701](#))
- Rezaei M., Solà Peracaula J., Malekjani M., 2022, [MNRAS](#), **509**, 2593
- Riess A. G., Casertano S., Yuan W., Bowers J. B., Macri L., Zinn J. C., Scolnic D., 2021, [ApJ](#), **908**, L6
- Rigault M., et al., 2015, [ApJ](#), **802**, 20
- Risaliti G., Lusso E., 2015, [ApJ](#), **815**, 33
- Risaliti G., Lusso E., 2019, [Nature Astronomy](#), **3**, 272
- Ryan J., Doshi S., Ratra B., 2018, [MNRAS](#), **480**, 759
- Ryan J., Chen Y., Ratra B., 2019, [MNRAS](#), **488**, 3844
- Sangwan A., Tripathi A., Jassal H. K., 2018, preprint, ([arXiv:1804.09350](#))
- Schöneberg N., Lesgourges J., Hooper D. C., 2019, [J. Cosmology Astropart. Phys.](#), **2019**, 029
- Scolnic D. M., et al., 2018, [ApJ](#), **859**, 101
- Simon J., Verde L., Jimenez R., 2005, [Phys. Rev. D](#), **71**, 123001
- Singh A., Sangwan A., Jassal H. K., 2019, [J. Cosmology Astropart. Phys.](#), **2019**, 047
- Sinha S., Banerjee N., 2021, [J. Cosmology Astropart. Phys.](#), **2021**, 060
- Solà Peracaula J., Gómez-Valent A., de Cruz Pérez J., 2019, [Physics of the Dark Universe](#), **25**, 100311
- Stern D., Jimenez R., Verde L., Kamionkowski M., Stanford S. A., 2010, [J. Cosmology Astropart. Phys.](#), **2**, 008
- Ureña-López L. A., Roy N., 2020, [Phys. Rev. D](#), **102**, 063510
- Vagnozzi S., Di Valentino E., Gariazzo S., Melchiorri A., Mena O., Silk J., 2021a, [Physics of the Dark Universe](#), **33**, 100851
- Vagnozzi S., Loeb A., Moresco M., 2021b, [ApJ](#), **908**, 84
- Wang J. S., Wang F. Y., Cheng K. S., Dai Z. G., 2016, [A&A](#), **585**, A68
- Wang F. Y., Hu J. P., Zhang G. Q., Dai Z. G., 2022, [ApJ](#), **924**, 97
- Wei J.-J., 2018, [ApJ](#), **868**, 29
- Wei J.-J., Melia F., 2022, [ApJ](#), **928**, 165
- Wu Q., Zhang G.-Q., Wang F.-Y., 2022, preprint, ([arXiv:2108.00581](#))
- Xu T., Chen Y., Xu L., Cao S., 2021, preprint, ([arXiv:2109.02453](#))
- Yang T., Banerjee A., Ó Colgáin E., 2020, [Phys. Rev. D](#), **102**, 123532
- Yu H., Ratra B., Wang F.-Y., 2018, [ApJ](#), **856**, 3
- Yu Z., et al., 2021, [MNRAS](#), **507**, 3771
- Zajaček M., et al., 2021, [ApJ](#), **912**, 10
- Zeng H., Yan D., 2019, [ApJ](#), **882**, 87
- Zhai Z., Blanton M., Slosar A., Tinker J., 2017, [ApJ](#), **850**, 183
- Zhang X., Huang Q.-G., 2021, [Phys. Rev. D](#), **103**, 043513
- Zhang C., Zhang H., Yuan S., Liu S., Zhang T.-J., Sun Y.-C., 2014, [Research in Astronomy and Astrophysics](#), **14**, 1221
- Zhang B. R., Childress M. J., Davis T. M., Karpenka N. V., Lidman C., Schmidt B. P., Smith M., 2017, [MNRAS](#), **471**, 2254
- Zhao D., Xia J.-Q., 2021, [European Physical Journal C](#), **81**, 694
- Zheng X., Cao S., Biesiada M., Li X., Liu T., Liu Y., 2021, [Science China Physics, Mechanics, and Astronomy](#), **64**, 259511

This paper has been typeset from a TeX/LaTeX file prepared by the author.